JACS
JOURNAL OF THE AMERICAN CHEMICAL SOCIETY

pubs.acs.org/JACS

Article

Rotation-Triggered Transmetalation on a Heterobimetallic Cu/Al *N*-Phosphine-Oxide-Substituted Imidazolylidene Complex

Takahiro Asada, Yoichi Hoshimoto,* and Sensuke Ogoshi*

Cite This: *J. Am. Chem. Soc.* 2020, 142, 9772–9784

Read Online

ACCESS | Metrics & More | Article Recommendations | Supporting Information

ABSTRACT: A novel strategy for the preparation of heterobimetallic *N*-heterocyclic carbene (NHC) complexes is demonstrated using *N*-phosphine-oxide-substituted imidazolylidenes (PoxIms). In these heterobimetallic Cu/Al complexes, the Cu and Al centers can be either completely separated or brought near each other via the rotation of the *N*-phosphinoyl group in the PoxIm ligands. Triggered by this rotation, transmetalation to exchange the Cu−O^{t}Bu and Al−C_6F_5 bonds occurs on *in situ*-generated Cu/Al PoxIm complexes, and the Cu−C_6F_5 and Al−O^{t}Bu bonds are formed in excellent yield. On the basis of the results of mechanistic studies, including the isolation/*in situ* observation of key complexes and theoretical calculations, a plausible reaction mechanism for an intramolecular transmetalation is proposed to proceed via an activation complex that includes the simultaneous coordination of the phosphinoyl oxygen atom to the Cu as well as the Al centers. Furthermore, the formation of carbon−carbon bonds between $Al(C_6F_5)_3$ and allyl bromide mediated/catalyzed by Cu/Al PoxIm complexes is demonstrated. Upon the consecutive transfer of three C_6F_5 groups from a single molecule of $Al(C_6F_5)_3$, allyl pentafluorobenzene derivatives were obtained. The present results demonstrate the role of phosphine oxide in the activation of organoaluminum reagents for the transmetalation between Cu(I) complexes bearing NHCs as well as the benefit of constructing an intramolecular system based on a heterobimetallic complex to achieve efficient transmetalation by programming the encounter of two organometallic fragments.

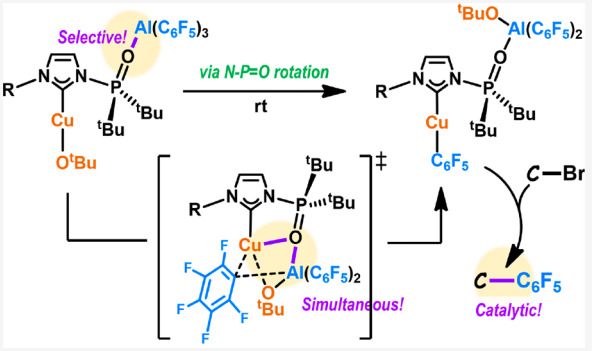

INTRODUCTION

Chemists have continuously devoted efforts to the discovery and development of multipurpose utility for known molecules. Indeed, numerous applications have been found for *N*-heterocyclic carbenes (NHCs) in diverse areas of chemistry.[1] Multifunctional NHCs equipped with additional coordination sites have further diversified the structure, reactivity, and applications of NHC-supported metal complexes by generating a variety of homo- and heteromultimetallic complexes.[2,3] Heterobimetallic NHC complexes are of particular interest in the fields of materials science[3l−n] and homogeneous catalysis,[3a−f] as the cooperative or synergetic roles of two metals have often afforded outcomes that are difficult to achieve using mononuclear organometallic or homobimetallic NHC complexes. It should thus be worthwhile to explore the unprecedented reactivity and utility of heterobimetallic NHC complexes by designing structurally defined multifunctional NHCs with dynamic behavior.

The reported procedures to selectively generate heterobimetallic NHC complexes can be classified into two types: stepwise metalation procedures that generally require the purification of a singly metalated product[3a,d,e,g,i,o] and ligand exchange procedures involving homobimetallic NHC complexes.[3c,f,j,k,m,n] In these examples, multifunctional NHC ligands, whose coordination sites are well-separated for the isolation of each metal center, are required to selectively generate heterobimetallic species (Figure 1A). However, this strategy to separate the metal centers from each other makes it fundamentally difficult to design molecular transformations that occur between these metal centers, such as transmetalation, which represents essential transformations in contemporary organometallic-based catalysis. Thus, a novel system that is able to strategically regulate the relative positions of two metal centers to allow them to be separated or brought together via reversible conformational change of the ligand would further expand the utility of the heterobimetallic NHC complexes (Figure 1B).

To achieve this goal, we envisioned the use of *N*-phosphine-oxide-substituted imidazolylidenes (PoxIms), which can predictably change their conformation (Scheme 1).[2i,4a,b] Under ambient conditions, PoxIms predominantly exist in the *anti*-conformation, in which the carbene carbon and the

Received: March 24, 2020
Published: April 20, 2020

https://dx.doi.org/10.1021/jacs.0c03252
J. Am. Chem. Soc. 2020, 142, 9772−9784

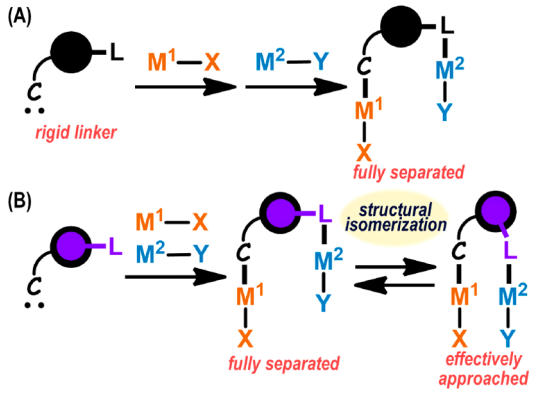

Figure 1. (A) Simplified representation of the reported procedures to afford heterobimetallic NHC complexes. (B) Design of a heterobimetallic NHC system in which two metal centers can be strategically separated or brought near one another.

Scheme 1. *N*-Phosphine-Oxide-Substituted Imidazolylidenes (PoxIms) and Imidazolinylidenes (SPoxIms) Used in This Work

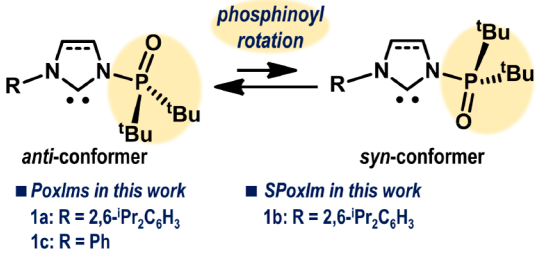

phosphinoyl oxygen atoms adopt an *anti*-orientation with respect to the N−P bond. Rotation of the *N*-phosphinoyl group to generate the *syn*-conformer can easily occur via a relatively low energy barrier ($\Delta E^{\ddagger} \sim 12$ kcal mol^{-1} for previously reported PoxIms).[4a] Four coordination modes have been reported in the complexation of metals with PoxIms: a κ-*O* and κ-*C* mode for *anti*-conformers[4a,e,g,h] as well as κ-*C* and κ-*C*,*O* modes for *syn*-conformers.[4a,d,f] As the carbene carbon and the phosphinoyl oxygen atoms in the *anti*-conformers are fully separated and expected to show distinctive reactivity, heterobimetallic complexes of the type (κ-*C*-M^1)(μ-PoxIm)-(κ-*O*-M^2) can be generated by a judicious choice of M^1 and M^2 (Scheme 2). Moreover, intramolecular transmetalation between the M^1−X and M^2−Y units should take place after effective approaches of them that are supported on *syn*-κ-*C*,*O*-PoxIm ligands. Herein, we report this type of transmetalation on heterobimetallic Cu/Al PoxIm complexes, in which the relative positions of the Cu−X and Al−Y fragments can be fully separated or made to approach one another (i.e., M^1 = Cu, M^2 = Al, X = O^{t}Bu/Br, Y = C_6F_5; Scheme 2). Mechanistic studies were also conducted in order to elucidate the roles of the *N*-phosphinoyl group. The use of the present system to develop a C−C bond-forming reaction between allyl bromide and Al(C_6F_5)$_3$ is also reported.

RESULTS AND DISCUSSION

Given the limited space around the carbene carbon atom in the *anti*-conformer of PoxIms,[4a] a choice of M^1 is key to the design of heterobimetallic PoxIm complexes (Scheme 2). Preferably, M^1 should exhibit a small covalent radius and form complexes with a low coordination number. These criteria prompted us to

Scheme 2. Strategy for the Preparation of Heterobimetallic M^1/M^2 Complexes Bearing (S)PoxIms and Subsequent Rotation-Triggered Transmetalation

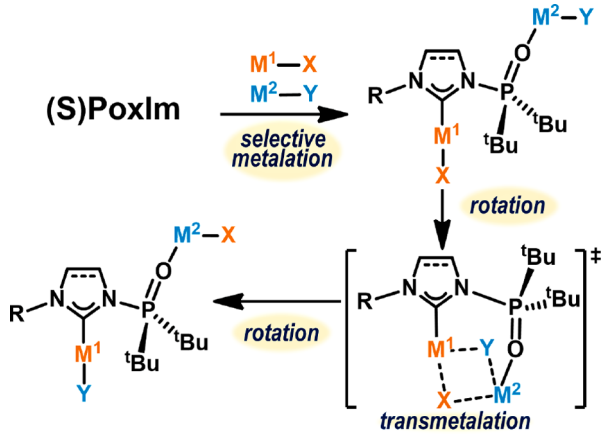

choose copper(I), which exhibits small covalent radii[5] and often affords two-coordinate Cu complexes bearing NHC and X ligands, wherein X is a neutral/anionic 2e$^-$ donor.[2m] On the other hand, M^2 should exhibit high oxophilicity (i.e., hard characteristics)[6a] for the selective complexation with the *N*-phosphinoyl oxygen atom. In this context, we have previously demonstrated that the *anti*-conformers of PoxIms form isolable complexes with Na$^+$ and Li$^+$ through a predominant coordination of the *N*-phosphinoyl moieties.[4e] The carbene moieties in these complexes remained intact and could thus be used as nucleophiles or Lewis bases in further reactions. Although a similar κ-*O*-PoxIm adduct with B(C_6F_5)$_3$ was characterized at −90 °C, it transformed into the thermodynamically stable carbene−B(C_6F_5)$_3$ adduct at room temperature.[4a] On the basis of these results, we employed Al(C_6F_5)$_3$ in this work, which should preferentially form a thermodynamically stable complex with the hard *N*-phosphinoyl oxygen atom rather than the softer carbene atom,[4h,6] while complexation between the carbene and Al(C_6F_5)$_3$ would still be possible.[7]

First, we experimentally confirmed the higher affinity of Al(C_6F_5)$_3$ toward the phosphine oxide than to B(C_6F_5)$_3$. For that purpose, we treated $Et_3P{=}O{\cdot}Al(C_6F_5)_3$ with B(C_6F_5)$_3$, but a reaction was not observed at room temperature (Scheme 3).[8]

Scheme 3. Comparison of the Reactivity of E(C_6F_5)$_3$ (E = B or Al) towards $Et_3P{=}O$

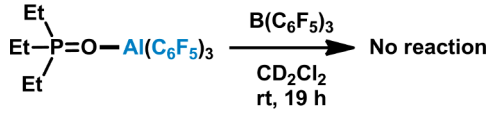

Subsequently, we examined the synthesis of heterobimetallic Cu/Al complexes using PoxIm **1a** (Figure 2A). Consecutive treatment of a toluene solution of **1a** at −30 °C with Al(C_6F_5)$_3$(tol)$_{0.5}$ (1.0 equiv) and CuO^{t}Bu (1.0 equiv) quantitatively afforded **2a**, which was isolated in >99% yield after 1.5 h. NMR and single-crystal X-ray diffraction analyses unambiguously confirmed the structure of **2a**, in which the carbene and the phosphinoyl moieties coordinate to the CuC_6F_5 and the Al(O^{t}Bu)(C_6F_5)$_2$ units, respectively. In the ^{31}P NMR spectrum of **2a**, a single resonance was observed at

https://dx.doi.org/10.1021/jacs.0c03252
J. Am. Chem. Soc. 2020, 142, 9772−9784

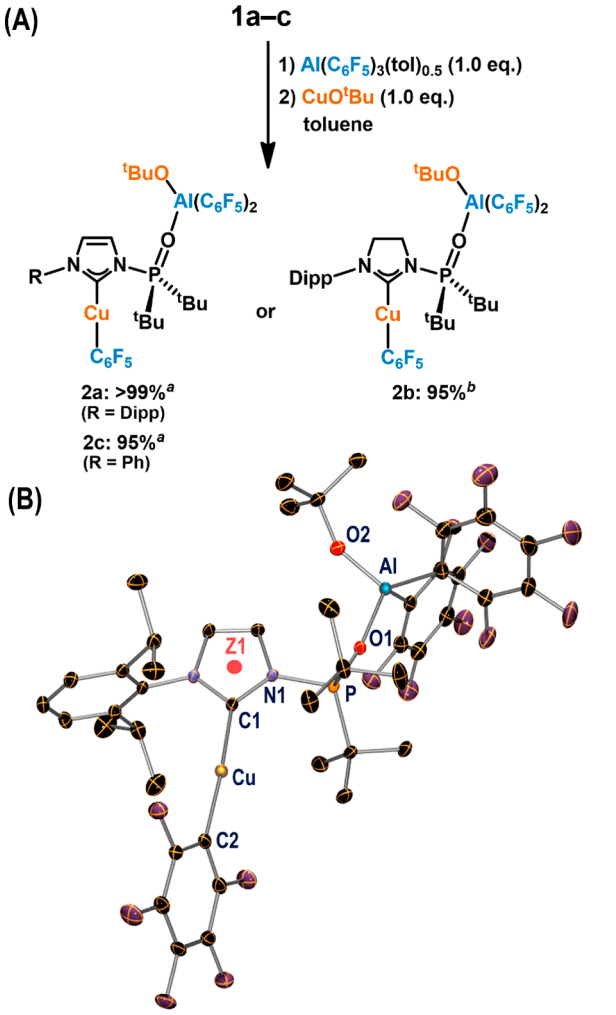

Figure 2. (A) One-pot, single-step synthesis of **2a**–**c**. Isolated yield of the products is shown. [a]The reaction mixture was initially kept at −30 °C (0.5 h) and subsequently allowed to warm to room temperature (1 h). [b]The reaction was conducted for 1 h at room temperature. (B) Molecular structure of **2a** with thermal ellipsoids at 30% probability; H atoms are omitted for clarity. Z1 represents the centroid of the imidazolylidene ring. Selected bond lengths [Å] and angles [°]: Cu–C1, 1.903(2); Cu–C2, 1.919(2); N1–P, 1.720(2); P–O1, 1.510(1); Al–O1, 1.814(2); Al–O2, 1.692(2); C1–N1–P–O1, 171.4(2); C1–Cu–C2, 173.76(9); P–O1–Al, 161.6(1).

84.0 ppm, which is downfield shifted relative to that of **1a** (δ_P = 63.0 in CD_2Cl_2). This result supports the notion that the phosphinoyl oxygen atom coordinates to a Lewis acid, which is consistent with the resonance of (κ-*O*-**1a**)$B(C_6F_5)_3$ at δ_P = 79.2 (−90 °C).[4a] Furthermore, the resonance corresponding to the carbene carbon atom of **2a** was observed at 183.9 ppm ($^2J_{C,P}$ = 20.0 Hz), which is almost identical to that of $IMesCuC_6F_5$ (δ_C = 181.2; IMes = 1,3-dimesitylimidazol-2-ylidene).[9a] The formation of **2a** was also supported by ^{19}F NMR analysis; i.e., the resonances for the C_6F_5 moieties bound to Cu and Al are observed at δ_F {−116.2, −163.7, −167.0} and δ_F {−125.1, −158.4, −165.9}, respectively. These NMR results are consistent with the molecular structure of **2a** determined by the single-crystal X-ray diffraction analysis (Figure 2B). These results thus demonstrate the transmetalation between the Cu–O^{t}Bu and Al–C_6F_5 bonds to afford Cu–C_6F_5 and Al–O^{t}Bu moieties. The solid-state structure of **2a** shows that the PoxIm moiety adopts an *anti*-conformation (∠C1–N1–P–O = 171.4(2)°), which enables the simultaneous coordination to the Cu and Al atoms in a (κ-*C*-Cu)(μ-**1a**)(κ-*O*-Al) fashion. The Al center adopts a tetrahedral coordination geometry though the coordination of the phosphinoyl oxygen atom (O1–Al = 1.814(2) Å). The P–O bond length in **2a** (1.510(1) Å) is longer than that in **1a** (1.482(1) Å); however, this P–O bond is still considered as a multiple bond, as it is shorter than the sum of the covalent bond radii of P (1.07 Å) and O (0.66 Å).[5] C1, Cu, and C2 are arranged in a nearly linear fashion (∠C1–Cu–C2 = 173.76(9)°). The CuC_6F_5 unit is located slightly out of ideal alignment with the carbene lone pair (∠Z1–C1–Cu = 172.4°; Z1 = centroid of the imidazolylidene ring), probably due to the high steric demand of the ^{t}Bu groups on phosphorus. On the other hand, in the solid-state structure of $IMesCuC_6F_5$, the three atoms corresponding to Z1, C1, and Cu in **2a** adopt an angle of 180°.[9a]

The transmetalation also proceeded when *N*-phosphine-oxide-substituted imidazolinylidene (SPoxIm) **1b**, which bears a *N*-2,6-^{i}Pr$_2$C$_6$H$_3$ (Dipp), or PoxIm **1c**, which bears a *N*-Ph moiety, were employed, affording heterobimetallic Cu/Al complexes **2b** and **2c** in 95% yields (Figure 2A). The molecular structures of **2b** and **2c** were determined by NMR and single-crystal X-ray diffraction analyses (**2b**, Figure S3; **2c**, Figure S4).[8]

The step-by-step preparation of **2a** was then carried out to gain insight into the mechanism underlying its formation (Figure 3A). The reaction of **1a** and $Al(C_6F_5)_3(tol)_{0.5}$ (1.0 equiv) in toluene afforded (κ-*O*-**1a**)$Al(C_6F_5)_3$ (**3a**) in 98% isolated yield within 1 h (−30 °C → room temperature). Similarly, **3b** was prepared in 95% yield via the complexation of **1b** and $Al(C_6F_5)_3(tol)_{0.5}$ (1.0 equiv) at room temperature. The molecular structures of **3a** and **3b** were unambiguously determined by NMR and single-crystal X-ray diffraction analyses (**3a**, Figure 3C; **3b**, Figure S6). In the ^{31}P NMR spectrum of **3a**, a resonance was observed at 80.5 ppm, which is almost identical to that of **2a** (*vide supra*). Importantly, the resonance of the carbene carbon atom of **3a** was observed at 220.9 ppm ($^2J_{C,P}$ = 34.8 Hz), which is almost identical to that of **1a** (δ_C = 220.5; $^2J_{C,P}$ = 25.0 Hz), whereas previously reported carbene–aluminum complexes showed resonances of the carbene carbons (δ_C) in the range of 169–181.[7] The ^{27}Al NMR spectrum of **3a** at −30 °C revealed a resonance at δ_{Al} = 117 ppm (brs), which is almost identical to that of $Et_3P{=}O{\cdot}Al(C_6F_5)_3$ (δ_{Al} = 112 ppm).[10] These results are consistent with a predominant complexation of $Al(C_6F_5)_3$ via the coordination of the *N*-phosphinoyl group in **1a**, which means that the carbene moiety remains available for a further complexation. The PoxIm moiety in **3a** adopts an *anti*-conformation in the solid state (Figure 3C), and the P–O1 and Al–O1 bond lengths are essentially identical when compared with those in **2a**. The reactions between **3a**/**3b** and CuO^{t}Bu (1.0 equiv) efficiently afforded **2a**/**2b** in 99% and 98% isolated yield, respectively. Thus, **3a**/**3b** would be involved as possible intermediates in the reactions shown in Figure 2A, given the identical reaction times for the quantitative formation of **2a**/**2b** from either **3a**/**3b** or **1a**/**1b**.

We also prepared (κ-*C*-**1a**)Cu(O^{t}Bu) (**4a**) via the reaction between **1a** and CuO^{t}Bu in toluene, and the structure of the product was again confirmed by NMR and X-ray crystallography (Figure 3A,D). There are two crystallographically independent molecules in the asymmetric unit of **4a**, albeit their structural parameters are essentially identical. The *anti*-

https://dx.doi.org/10.1021/jacs.0c03252
J. Am. Chem. Soc. 2020, 142, 9772–9784

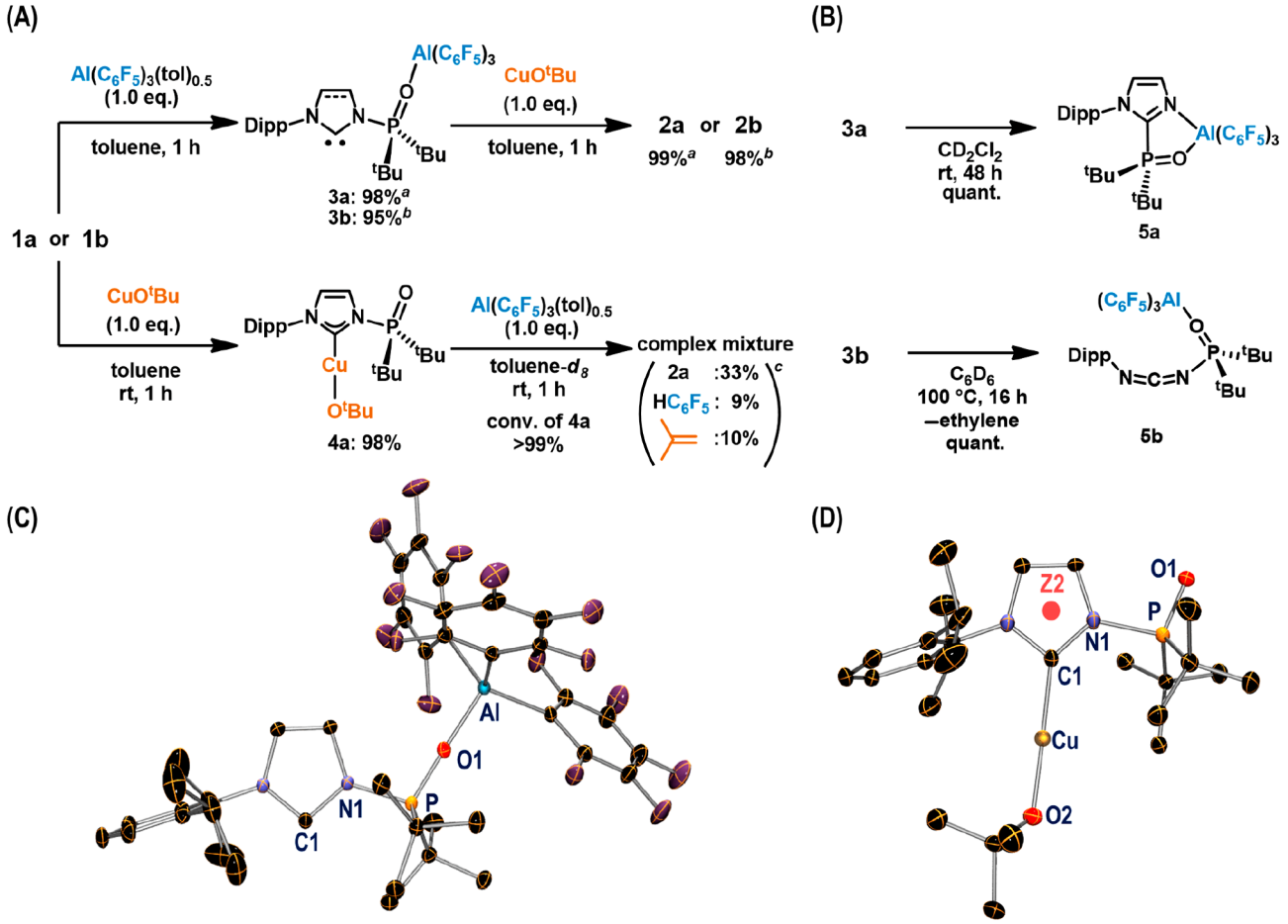

Figure 3. (A) Synthesis of **3a**/**3b** and **4a** and subsequent conversion into **2a**. Isolated yield of the products is shown. [a]The reaction mixture was initially kept at −30 °C and then allowed to warm to room temperature. [b]The reaction was conducted at room temperature. [c]The yield was determined by NMR analysis. (B) Transformation of **3a**/**3b** to **5a**/**5b**. Yield was confirmed by NMR analysis. Molecular structures of (C) **3a** and (D) **4a** (extracted from two crystallographically independent molecules in the asymmetric unit) with thermal ellipsoids at 30% probability; H atoms and solvate molecules for **3a** (toluene) and **4a** (THF) are omitted for clarity. Z2 represents the centroid of the imidazolylidene ring. Selected bond lengths [Å] and angles [°] for **3a**: N1−P, 1.696(2); P−O1, 1.515(1); Al−O1, 1.791(1); P−O1−Al, 177.3(1); C1−N1−P−O, 174.6(2); **4a**: Cu−C1, 1.872(6); Cu−O2, 1.811(4); N1−P, 1.771(5); P−O1, 1.483(4); C1−N1−P−O1, 172.1(5); C1−Cu−O2, 178.9(2).

conformation of the PoxIm moiety was observed in the crystalline lattice of **4a**. Steric repulsion between the CuO^{t}Bu and ^{t}Bu groups in **4a** is again confirmed by the nonlinear arrangement of Z2, C1, and Cu (171.8°; Z2 = centroid of the imidazolylidene ring). Subsequently, the preparation of **2a** by treating **4a** with $Al(C_6F_5)_3(tol)_{0.5}$ (1.0 equiv) in toluene-d_8 at room temperature was monitored by ^{1}H, ^{31}P, and ^{19}F NMR spectroscopy (Figures S15 and S16). The complex **4a** was consumed within 5 min, and a complex mixture including **2a** (33%), HC_6F_5 (9%), and isobutene (10%) was obtained after 1 h. These results imply that the abstraction of the O^{t}Bu moiety by $Al(C_6F_5)_3$ causes the decomposition of **4a** to produce the aforementioned byproducts. This decomposition would compete with the coordination of the *N*-phosphinoyl oxygen atom in **4a** to $Al(C_6F_5)_3$, which eventually yielded **2a**. The selective coordination of the carbene and *N*-phosphinoyl moieties in **1** to the Cu and Al center, respectively, is thus essential for the spatial separation of these metals to prevent side reactions as well as the subsequent transmetalation to afford **2**.

The thermal stability of **3a** and **3b** was also evaluated. At room temperature, the phosphinoyl moiety in **3a** gradually migrated to the carbene atom,[11a] yielding the penta-coordinated aluminum complex **5a**, which bears three C_6F_5 ligands (Figure 3B). In light of the fact that this decomposition proceeds at room temperature, the reaction between **3a** and CuO^{t}Bu should be initiated below room temperature, e.g., at −30 °C as shown in Figure 2A. Note that **1a** decomposed in less than 10% when heated even at 100 °C for 24 h in the absence of $Al(C_6F_5)_3$. The complex **3b** showed much higher stability; i.e., only 6% of **3b** decomposed after 48 h at room temperature. A thermolysis of **3b** (100 °C; 16 h) resulted in the formation of **5b**, in which an *N*-phosphinoyl-substituted carbodiimide coordinates to the Al center via the generation of ethylene (confirmed by ^{1}H NMR).[11b] The molecular structures of both **5a** and **5b** were determined by X-ray crystallography and are shown in Figures S8 and S10, respectively.

To clarify the impact of the complexation on the activation energy barrier of the rotation of the *N*-phosphinoyl moiety ($\Delta E^{\ddagger}$), DFT calculations were conducted using **1c**, (*κ*-*O*-**1c**)$Al(C_6F_5)_3$ (**3c**), and (*κ*-*C*-**1c**)Cu(O^{t}Bu) (**4c**) as model compounds (Figure 4). The introduction of $Al(C_6F_5)_3$ on the *N*-phosphinoyl group resulted in a decrease of the activation energy barrier for the rotation in **3c** ($\Delta E^{\ddagger}$ = +10.1 kcal·mol^{-1}) relative to that of **1c** ($\Delta E^{\ddagger}$ = +12.9 kcal·mol^{-1}). In addition, the

https://dx.doi.org/10.1021/jacs.0c03252
J. Am. Chem. Soc. 2020, 142, 9772−9784

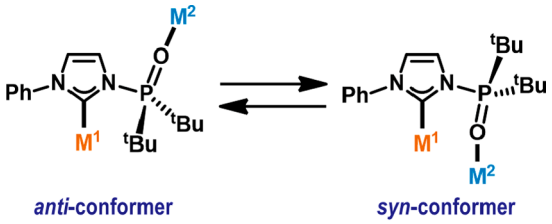

compound (M^1, M^2)	$\Delta E^{\ddagger}$ ($\Delta G^{\ddagger}$)	ΔE° (ΔG°)
1c (none, none)	+12.9 (+13.9)	+9.0 (+9.2)
3c (none, $Al(C_6F_5)_3$)	+10.1 (+11.3)	+4.1 (+5.0)
4c (CuO^tBu, none)	+19.3 (+20.5)	+8.5 (+8.6)

Figure 4. Activation energy barriers for the rotation of the *N*-phosphinoyl moiety ($\Delta E^{\ddagger}$, kcal·mol^{-1}) and relative free energies of the *syn*-conformer with respect to the *anti*-conformer (ΔE°, kcal·mol^{-1}) in **1c**, **3c**, and **4c**. DFT calculations were conducted at the ωB97X-D/SDD for Cu and 6-311G(d,p) for others//LanL2DZ for Cu and 6-31G(d) for others (gas phase, 25 °C). C1−N1−P−O angles [°] for *anti*-**1c**: 172.0; *syn*-**1c**: 35.9; *anti*-**3c**: 178.5; *syn*-**3c**: 56.9; *anti*-**4c**: 172.1; *syn*-**4c**: 18.9.

difference between the relative free energies of the *anti*- and *syn*-conformers (ΔE°) also decreased in **3c** (ΔE° = +4.1 kcal·mol^{-1}) relative to **1c** (ΔE° = +9.0 kcal·mol^{-1}). The C−N−P−O torsion angles are clearly different in the optimized structures of the *syn*-conformers of **1c** (35.8°) and **3c** (56.9°), which should be rationalized in terms of the steric repulsion generated between the *N*-Ph group and the $Al(C_6F_5)$ moiety in the latter case. It should also be noted that the C−N−P−O angles are almost identical for the *anti*-conformers (**1c**: 172.0°; **3c**: 178.4°) and TS structures (**1c**: 83.4°; **3c**: 83.5°). In the case of **3c**, H···F interactions (ca. 2.5 Å)[12] were observed between the *N*-Ph and C_6F_5 groups in the TS structure and the *syn*-conformer, which should contribute to their stabilization. In stark contrast, in the case of **4c**, the introduction of CuO^tBu on the carbene carbon destabilized the activation complex for the rotation of the *N*-phosphinoyl group ($\Delta E^{\ddagger}$ = +19.3 kcal·mol^{-1}) due to the steric repulsion between the CuO^tBu unit and the ^{t}Bu groups. These results show that the activation energy barrier for the rotation of the *N*-phosphinoyl moieties in PoxIms can be tuned via the introduction of metals (or Lewis acids) on the carbene carbon or phosphinoyl oxygen atoms; however, the *anti*-conformer predominates in both cases, at least under the conditions applied.

Next, the reaction between **3a** and CuO^tBu in C_6D_6 at 22 °C was monitored by ^{1}H, ^{19}F, and ^{31}P NMR spectroscopy (Figure 5A). After 30 min, the total consumption of **3a** and the formation of **2a** (31%), **6a** (15%), and **7a** (24%) were observed. The yield of **2a** increased to 82% after 1 h, and some unidentified resonances were observed in the ^{19}F NMR spectrum. The *in situ* generation of **6a** and **7a** was proposed on the basis of their characteristic ^{31}P NMR resonances, i.e., δ_P = 64.4 (**6a**) and 87.4 (**7a**). The former value is slightly downfield shifted with respect to that of **1a** (δ_P = 61.4 in C_6D_6), which suggests that this phosphinoyl moiety does not engage in a donor−acceptor interaction with Al species, while the latter shows the complexation between its phosphinoyl

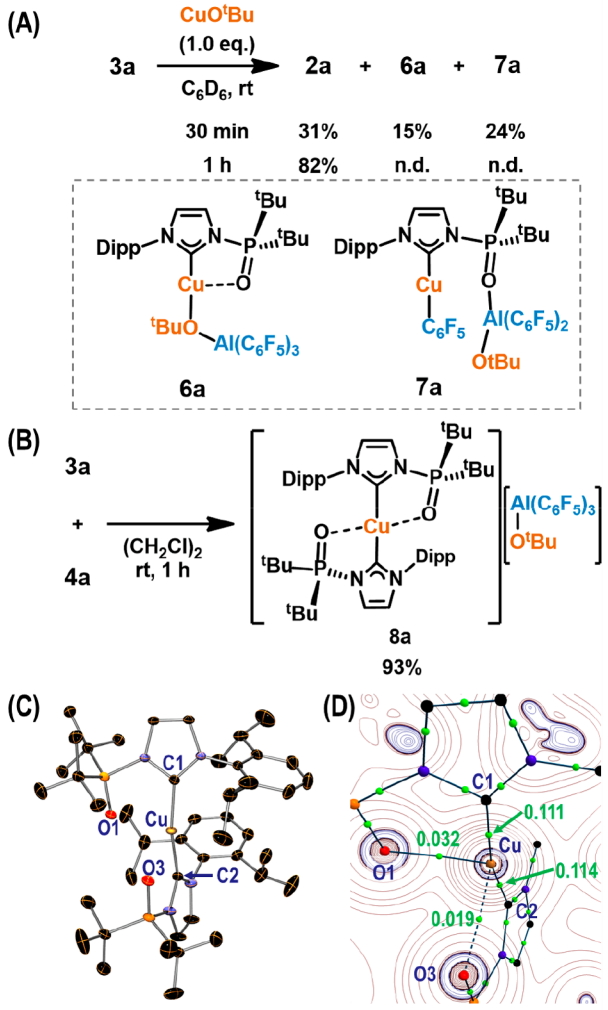

Figure 5. (A) Monitoring the reaction between **3a** and CuO^tBu by NMR spectroscopy. Yield was determined by ^{19}F NMR analyses using $PhCF_3$ as an internal standard. (B) Isolation of **8a** (isolated yield). (C) Molecular structure of the cationic moiety in **8a**; thermal ellipsoids at 30% probability; H atoms omitted for clarity. (D) The quantum theory of AIM bond paths and bond critical points (green dots; selected electron density in $e \times r_{Bohr}^{-3}$) in the cationic unit in **8a** with overlaid contour plots of $\nabla^2\rho$ through the plane defined by the Cu, O1, and O3 atoms. Selected atoms and values of electron density on the selected bond critical points are shown.

oxygen atom and the Al species. In addition, in the case of **7a**, characteristic resonances for the CuC_6F_5 and $Al(C_6F_5)_2$ moieties were observed at −116.1, −161.8, and −165.5 ppm as well as at −124.1, −155.0, and −164.2 ppm, respectively, in their ^{19}F NMR spectra, which are almost identical to those of **2a** (*vide supra*). These results and those of the theoretical studies shown in Figure 6A are consistent with the formation of **6a** and **7a**. The isolation of these complexes was hampered by their conversion to **2a** even at −20 °C. We thus turned our attention to capture *in situ*-generated **6a** in the presence of an additional Lewis base via a ligand substitution reaction. When **3a** was treated with **4a** in 1,2-dichloroethane, **8a** was isolated in 93% yield (Figure 5B). The molecular structure of **8a** was determined on the basis of NMR, HRMS, and single-crystal X-ray diffraction analyses (Figure 5C). In the solid-state structure of the cationic part of **8a**, the interatomic distance of Cu···O1 (2.399(2) Å) is shorter than that of Cu···O3 (2.680(2) Å).

https://dx.doi.org/10.1021/jacs.0c03252
J. Am. Chem. Soc. 2020, 142, 9772−9784

This unsymmetrical structure in $[(\kappa\text{-}C,O\text{-}\mathbf{1a})_2Cu]^+$ was closely reproduced in the gas-phase optimized structure of the isolated cationic part of **8a** at the ωB97X-D/6-31+G(d,p) level of theory (Cu···O1 = 2.44 Å; Cu···O3 = 2.53 Å). To clarify a participation of bonding interactions between these atoms, a topological analysis of the electron density (ρ) was performed on the basis of the quantum theory of atoms in molecules (AIM) method[13a,b] using the structural parameters obtained from the single-crystal X-ray diffraction analysis. The bond paths (solid and dashed lines), bond critical points (green dots), and the contour plots of the Laplacian of ρ ($\nabla^2\rho$) through the plane defined by the Cu, O1, and O3 atoms are shown in Figure 5D. Larger values in ρ ($0.032e \times r_{Bohr}^{-3}$), $\nabla^2\rho$ ($+0.119e \times r_{Bohr}^{-3}$), and the delocalization index (δ(Cu,O1) = 0.20 based on the SCF density) were observed at the bond critical point between Cu and O1 relative to those between Cu and O3 (ρ = $0.019e \times r_{Bohr}^{-3}$; $\nabla^2\rho$ = $+0.064e \times r_{Bohr}^{-3}$; δ(Cu,O3) = 0.12), supporting the existence of a stronger donor–acceptor interaction in the former case.[14] The cationic Cu center would thus be stabilized by the coordination of O1. In solution, a single resonance at 64.5 ppm is observed in the ^{31}P NMR spectrum, indicative of a facile coordinative exchange between O1 and O3. It should also be noted here that the resonances observed in the ^{31}P and ^{19}F NMR spectra of **8a** are closely related to those of **6a**, which corroborates the *in situ* formation of **6a** (Figure 5A); however, **8a** was not converted into **2a**, even after 2 days at room temperature.

To confirm the role of the phosphine oxide and the benefits of the intramolecular system in the present transmetalation, control experiments were conducted (Scheme 4). The reaction

Scheme 4. Control Experiments[a]

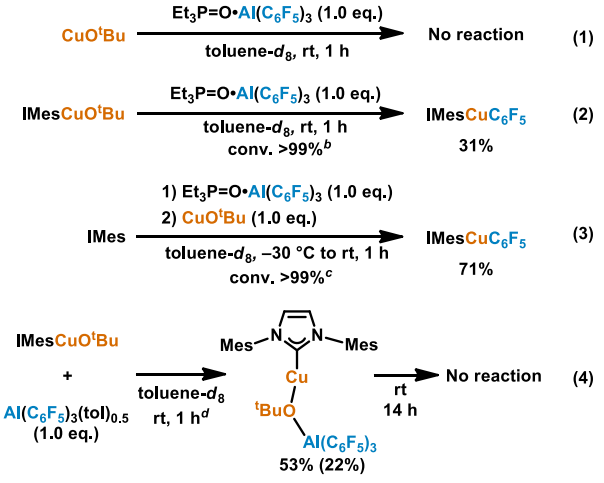

[a]Yield was determined by ^{1}H and ^{19}F NMR analyses using $PhCF_3$ as an internal standard. Isolated yield was given in parentheses. [b]A complex mixture including HC_6F_5 (12%) was obtained. [c]A complex mixture including HC_6F_5 (5%) was obtained. [d]HC_6F_5 (32%) was also obtained.

systems were opened under an N_2 atmosphere when $PhCF_3$ was added as an internal standard prior to transferring the reaction mixture to the NMR tubes. Thus, a gaseous byproduct, e.g., isobutene, was not observed in the following NMR analyses, even if generated *in situ*. A reaction did not occur when CuO^{t}Bu was treated with $Et_3P{=}O{\cdot}Al(C_6F_5)_3$ at room temperature for 1 h (eq 1, Scheme 4). In contrast, $IMesCuC_6F_5$ was formed in 31% yield when *in situ*-generated IMesCuO^{t}Bu and $Et_3P{=}O{\cdot}Al(C_6F_5)_3$ were reacted in toluene-d_8 at room temperature (eq 2, Scheme 4). Although the resultant mixture was complex, the complete consumption of IMesCuO^{t}Bu and the formation of HC_6F_5 (12%) were confirmed. We optimized the conditions for the intermolecular transmetalation between IMesCuO^{t}Bu and $Al(C_6F_5)_3$ and found that the consecutive addition of $Et_3P{=}O{\cdot}Al(C_6F_5)_3$ and CuO^{t}Bu to the toluene-d_8 solution of IMes at −30 °C improved the yield of $IMesCuC_6F_5$ to 71% (eq 3, Scheme 4). When $Al(C_6F_5)_3(tol)_{0.5}$ was employed in the reaction with IMesCuO^{t}Bu, $[IMesCu(\mu\text{-}O^tBu)Al(C_6F_5)_3]$ was furnished in 53% as a major product with the concomitant generation of HC_6F_5 in 32% (eq 4, Scheme 4). The molecular structure of $[IMesCu(\mu\text{-}O^tBu)Al(C_6F_5)_3]$ was characterized by NMR and single-crystal X-ray diffraction analyses, and the latter is shown in Figure S13. Importantly, no reaction occurred from $[IMesCu(\mu\text{-}O^tBu)Al(C_6F_5)_3]$ within 14 h at room temperature. Thermolysis of $[IMesCu(\mu\text{-}O^tBu)Al(C_6F_5)_3]$ at 80 °C for 1 h resulted into its decomposition, whereas the formation of $IMesCuC_6F_5$ was not observed. These results demonstrate the following points: (i) an additional ligand for Cu is essential for the transmetalation between $Al(C_6F_5)_3$ under the applied conditions, and NHCs are appropriate in this context. (ii) The addition of phosphine oxide effectively promotes the transmetalation between the Cu–heteroatom and Al–C bonds, while the generation of organoaluminate species upon the addition of Lewis bases such as alkyl amido anions, carbanions, or Cl^- has been reported to be critical in the reported examples.[15] (iii) One critical benefit of constructing such intramolecular heterobimetallic systems rather than intermolecular systems is their excellent efficiency to afford the transmetalated products (e.g., Figure 2A vs eq 3 in Scheme 4), as the collision of Cu–O^{t}Bu and Al–C_6F_5 moieties should be preprogrammed under such intramolecular conditions.

Both inter- and intramolecular transmetalation pathways can compete for the formation of **2** in the reaction of **1**, $Al(C_6F_5)_3$, and CuO^{t}Bu. Nevertheless, the formation of **2** via the complexation between **3** and CuO^{t}Bu should predominantly occur in an intramolecular fashion that proceeds via intermediates such as **6a** and **7a**, considering the results of the aforementioned experiments as well as the following DFT calculations. A plausible mechanism for the formation of **2c** via the complexation between **3c** and CuO^{t}Bu is proposed in Figure 6A. DFT calculations were carried out at the ωB97X-D/SDD for Cu and 6-311G(d,p) for others//LanL2DZ for Cu and 6-31G(d) for others. The relative Gibbs free energies with respect to **I** (0.0 kcal·mol^{-1}) are also given in Figure 6A. Initially, the complexation between the carbene carbon atom of **3c** and CuO^{t}Bu gives rise to the formation of **I**. A rotation of the *N*-phosphinoyl moiety via **TS1** (+15.5 kcal·mol^{-1}) and a subsequent intramolecular coordination of the O^{t}Bu unit to the Al center furnishes transient intermediate **II** (+2.4 kcal·mol^{-1}), which involves a penta-coordinated Al center. The intermediate **II** is converted into *syn*-**III** (−21.9 kcal·mol^{-1}) without an activation energy barrier. Isomerization between *syn*-**III** and *anti*-**III** (−20.4 kcal·mol^{-1}) can participate in the reaction system; however, the subsequent transmetalation occurs from thermodynamically favorable *syn*-**III**. The formation of *syn*-**III** might also be possible via *anti*-**III**, which is generated via an intermolecular $Al(C_6F_5)_3$ transfer between two molecules of **I**; however, at present, we do not consider that this path is plausible, as the reaction between **4a** and $Al(C_6F_5)_3(tol)_{0.5}$ resulted in the formation of a complex

https://dx.doi.org/10.1021/jacs.0c03252
J. Am. Chem. Soc. 2020, 142, 9772–9784

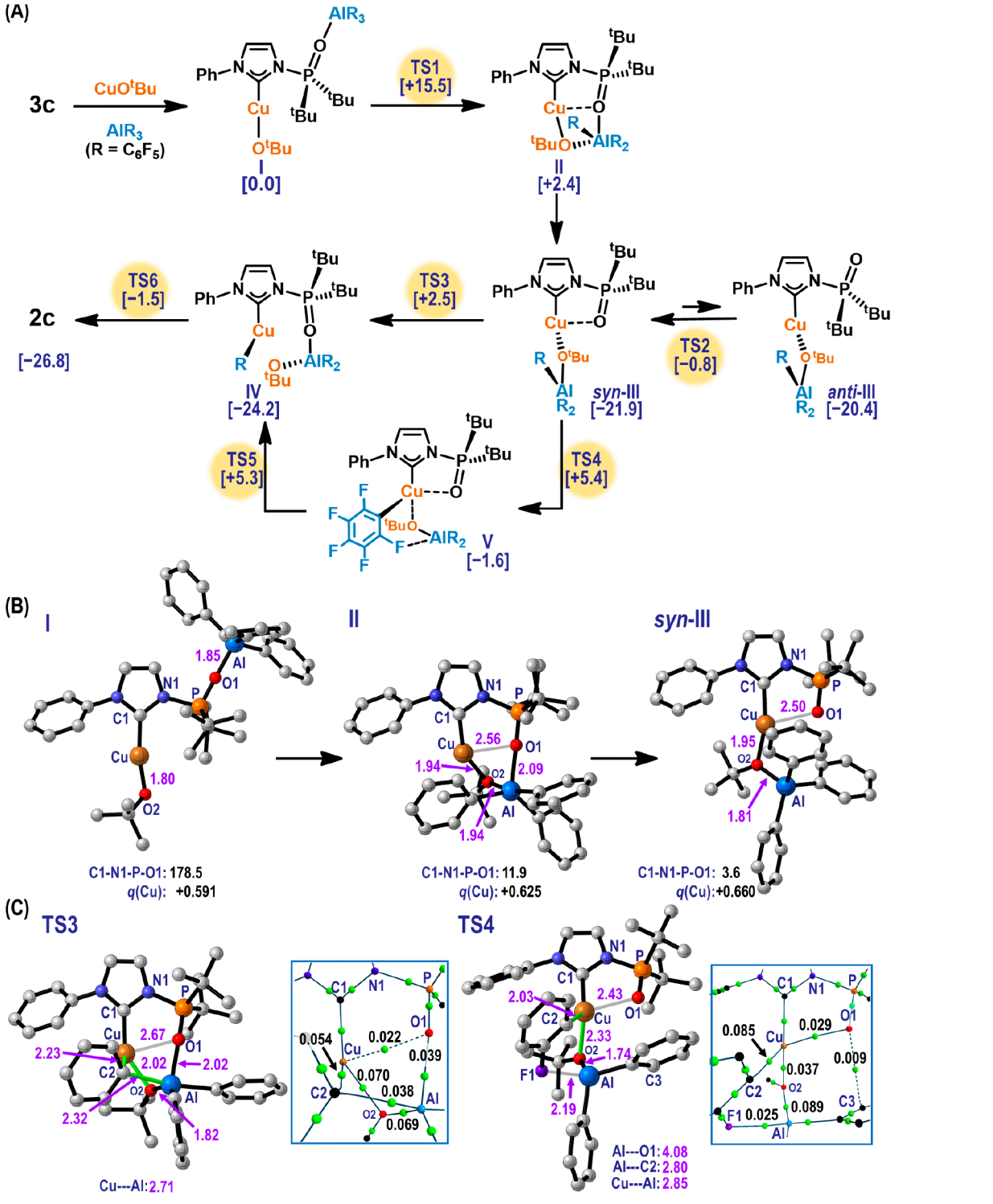

Figure 6. (A) Plausible mechanisms for the formation of **2c** from **3c**. Relative Gibbs free energies [kcal·mol^{-1}] with respect to **I** [0.0] are shown; these values were calculated by DFT using the ωB97X-D/SDD for Cu and 6-311G(d,p) for others//LanL2DZ for Cu and 6-31G(d) for others. (B) Optimized molecular structures for **I**, **II**, and *syn*-**III**. Selected distances between two atoms [Å], C1−N1−P−O1 torsion angle [°], and atomic charges on Cu, q(Cu) [$e \times r_{Bohr}^{-3}$] are also shown. (C) Optimized molecular structures for **TS3** and **TS4**. Transient bonds in **TS3** (Cu···C2, C2···Al, Cu···O2) and in **TS4** (Cu···C2, Cu···O2) are shown in light green solid lines. For each structure, the selected bond paths (solid/dashed lines), bond critical points (green dots), and electron density [$e \times r_{Bohr}^{-3}$] at these bond critical points are also shown.

mixture, even though this reaction can directly generate [(κ-C-**1a**)Cu(μ-O^{t}Bu)Al(C$_6$F$_5$)$_3$] (Figure 3A). From *syn*-**III**, two paths for the intramolecular transmetalation were explored; on one hand, transmetalation could occur via an activation complex **TS3** (+2.5 kcal·mol^{-1}) that includes the coordination of the phosphinoyl oxygen to the Al center; on the other hand, transmetalation could occur via **TS4** (+5.4 kcal·mol^{-1}) without an interaction between Al and O1. The former path via **TS3** directly affords intermediate **IV** (−24.2 kcal·mol^{-1}), while the migration of the Al(C$_6$F$_5$)$_2$(O^{t}Bu) moiety from **V** (−1.6 kcal·

https://dx.doi.org/10.1021/jacs.0c03252
J. Am. Chem. Soc. 2020, 142, 9772−9784

mol^{-1}) via **TS5** (+5.3 kcal·mol^{-1}) is involved in the latter case. Intermediate **IV** is a *syn* conformer of the product **2c** (−26.8 kcal·mol^{-1}), and the rotation of the phosphinoyl moiety thus converts **IV** into **2c** via **TS6** (−1.5 kcal·mol^{-1}). The coordination of O1 to the Cu centers in **II**, *syn*-**III**, **V**, and **TS3**−**5** are proposed on the basis of the AIM analyses of their gas-phase optimized structures. The overall process to give **2c** from **I** is energetically favorable (ΔG° = −26.8 kcal·mol^{-1}). The highest activation energy barrier for the mechanism via **TS3** is estimated to be +24.4 kcal·mol^{-1}, which is 2.9 kcal·mol^{-1} less than the paths via **TS4** ($\Delta G^\ddagger$ = +27.3 kcal·mol^{-1}). The path via **TS3** is thus kinetically preferable and predominant, albeit both paths can compete at ambient temperature. The observation of **6a** and **7a** (Figure 5A), which are closely related to *syn*-**III** and **IV**, respectively, is consistent with the proposed mechanism.

In Figure 6B, the optimized molecular structures of **I**, **II**, and *syn*-**III** are shown together with selected structural parameters and atomic charges on Cu (q(Cu), $e \times r_{Bohr}^{-3}$; estimated on the basis of the AIM analysis). During the formation of *syn*-**III** from **I**, the phosphinoyl moiety rotates by ca. 175°, which changes the relative position of the Al atom with respect to the Cu atom. The coordination of O2 to Al causes an elongation of the Cu−O2 bond (1.80 Å in **I** → 1.95 Å in *syn*-**III**), which results in an increase of the cationic character of the Cu center (q(Cu): +0.591$e \times r_{Bohr}^{-3}$ in **I** → +0.660$e \times r_{Bohr}^{-3}$ in *syn*-**III**). These cationic Cu centers in **II** and *syn*-**III** are thermodynamically stabilized by the coordination of O1, similarly to that observed in **8a**.

To gain further insights into the role of the phosphinoyl moieties in the transmetalation events, the optimized molecular structures and bonding situation (bond paths and electron density at the bond critical points) were compared between **TS3** and **TS4** (Figure 6C). For the AIM analysis, single-point calculations were carried out at the ωB97X-D/Def2SVP level of theory. The interatomic distance between the Cu and Al atoms significantly decreases in **TS3** (2.71 Å) and **TS4** (2.85 Å) compared to that in **I** (6.85 Å). Especially the value in **TS3** is nearly identical to the sum of the covalent radii of Cu and Al (2.53 Å);[5] however, a bond critical point was not found between these atoms. A longer interatomic distance (2.67 Å in **TS3** vs 2.43 Å in **TS4**) as well as a decreased electron density at the bond critical point (0.022$e \times r_{Bohr}^{-3}$ in **TS3** vs 0.029$e \times r_{Bohr}^{-3}$ in **TS4**) suggest a weaker interaction between Cu and O1 in **TS3** compared to **TS4**. In **TS3**, the formation of the Cu−C2 bond (2.23 Å) and the cleavage of the Cu−O2 (2.02 Å) and C2−Al (2.32 Å) bonds occur simultaneously. Moreover, a coordination of O1 to the Al center is clearly involved. In contrast, the bond exchange between the Cu−O^{t}Bu and Al−C_6F_5 units seems to be almost complete in **TS4** (Cu−C2 = 2.03 Å; C2···Al = 2.80 Å); a bond path was not found between C2 and Al. Similarly, a bond path was not observed between the O1 and Al atoms in **TS4**. Instead, we observed an interaction between F1 and Al (F1−Al = 2.19 Å; ρ = 0.025$e \times r_{Bohr}^{-3}$ at the corresponding bond critical point), which is consistent with the optimized structure of **V**. The aforementioned theoretical results manifest that the phosphinoyl moieties play a key role in stabilizing the cationic Cu centers during these transition states. In addition, especially in the predominant path via **TS3**, the phosphinoyl moiety contributes to facilitate the preferable arrangement of the Cu, C2, Al, and O2 atoms as well as to activate the Al−C_6F_5 units for the smooth progress of the transmetalation at ambient temperature.

Chang and co-workers.[9a,b] as well as others[16] have extensively studied the utility of CuC_6F_5 complexes bearing NHC ligands in C−C bond-forming reactions, for example, the allylation of polyfluoroarenes with allyl bromide. Encouraged by these pioneering results, we attempted to apply the present system to the unprecedented C−C bond formation between allyl bromide and $Al(C_6F_5)_3$ (Figure 7A). In the presence of an equimolar amount of CuO^{t}Bu and **1a** relative to $Al(C_6F_5)(tol)_{0.5}$, i.e., 0.33 equiv per C_6F_5 unit, the transfer of three C_6F_5 groups from a single molecule of $Al(C_6F_5)_3$ to allyl bromide (3.5 equiv) proceeded to afford allyl pentafluorobenzene in 68% yield (run 1, Figure 7A). The treatment of allyl bromide with $Al(C_6F_5)_3(tol)_{0.5}$ resulted in the oligomerization of allyl bromide, while allyl pentafluorobenzene was not produced. Employing **1b**, **1c**, and IMes also afforded allyl pentafluorobenzene in 65%, 78%, and 42% yield, respectively (runs 2−4, Figure 7A), and **1c** was thus used for the further optimization of the reaction conditions. It is noteworthy that the precipitation of single crystals from the reaction solutions was observed for runs 1−3, Figure 7A. In run 3 (Figure 7A), single crystals were isolated in 24% yield by filtration, and the molecular structure of **15c** was determined unequivocally by ESI-MS and single-crystal X-ray diffraction analyses (Figure 8A; *vide infra*). Increasing the amount of allyl bromide to 5.0 equiv resulted in the formation of allyl pentafluorobenzene in 93% yield (run 5, Figure 7A). When cinnamyl bromide (5.0 equiv) was employed, the formation of C−C bonds proceeded at both the α- and γ-positions in a 48:52 ratio to afford allyl pentafluorobenzene derivatives in >99% total yield (run 6, Figure 7A).

We then explored the stepwise transformation of **2c** with allyl bromide (Figure 7B). The first C−C bond-forming reaction between **2c** and allyl bromide occurred at room temperature to quantitatively afford allyl pentafluorobenzene and (**9c**)$_2$. The dimeric structure of (**9c**)$_2$ was confirmed by a single-crystal X-ray diffraction analysis (Figure S14). Complex (**9c**)$_2$ did not react with allyl bromide (1.05 equiv per C_6F_5 units) at room temperature, and heating at 80 °C was required for the further progress of the reaction, which afforded additional allyl pentafluorobenzene quantitatively based on a molar amount of the C_6F_5 groups in (**9c**)$_2$. Moreover, we observed the concomitant production of the complexes (**13c**)$_2$ and (**14c**)$_2$ in 64% and 6%, respectively, relative to (**9c**)$_2$. The molecular structures of (**13c**)$_2$ and (**14c**)$_2$ were determined on the basis of ^{1}H, ^{13}C, and ^{31}P NMR spectroscopic analyses, and a preliminary X-ray diffraction analysis of (**13c**)$_2$ confirms the aforementioned identification (Figure S29). The formation of (**13c**)$_2$ could be rationalized by the following reaction sequences: (i) the transmetalation between the Cu−Br and Al−C_6F_5 bonds in monomeric **9c** could result in the formation of **10c** including (κ-*C*-**1c**)CuC_6F_5 and (κ-*O*-**1c**)Al(O^{t}Bu)(Br)(C_6F_5) moieties, followed by a C−C bond formation between allyl bromide to give **11c** including a (κ-*C*-**1c**)CuBr unit; (ii) the consecutive transmetalation/C−C bond-forming reactions could take place again to eventually afford **13c** from **11c** via **12c**; (iii) a disproportionation of the O^{t}Bu and Br ligands in **13c** would result in the formation of a mixture of **13c** and **14c**, which was independently confirmed by the reaction among **1c**, $AlBr_3$ and CuO^{t}Bu (Figures S26−28). Although the reaction of (**9c**)$_2$ with allyl bromide was monitored by NMR spectroscopy, the *in situ* generation of (**10c**)$_n$−(**12c**)$_n$ (n = 1 and/or 2) was

https://dx.doi.org/10.1021/jacs.0c03252
J. Am. Chem. Soc. 2020, 142, 9772−9784

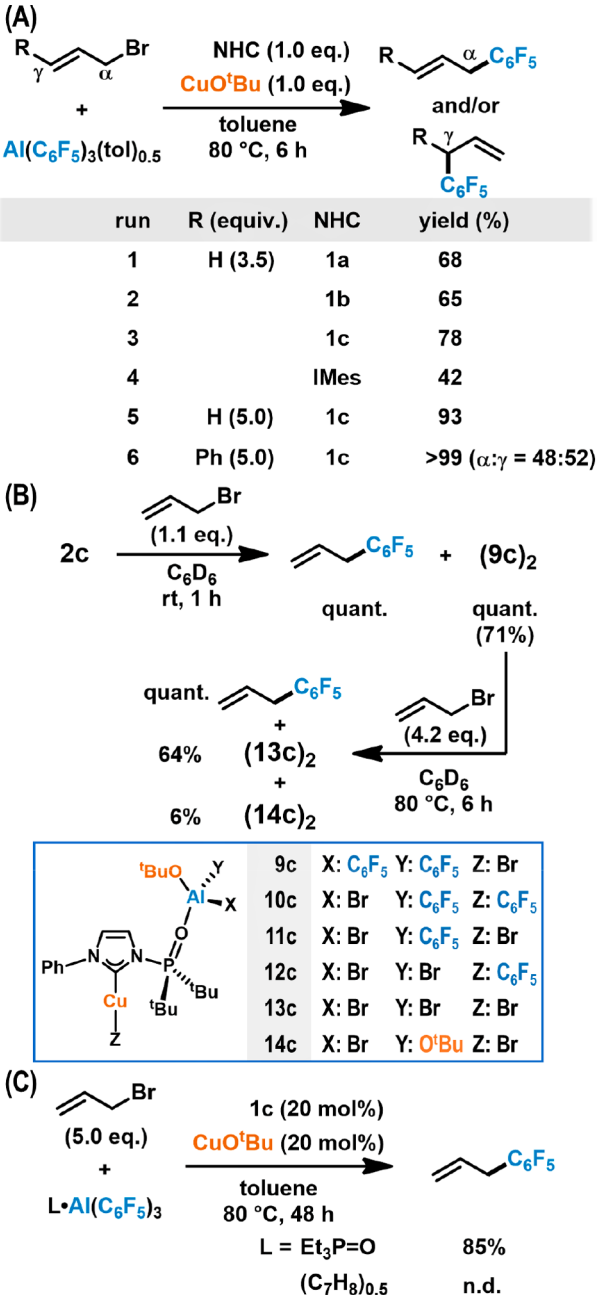

run	R (equiv.)	NHC	yield (%)
1	H (3.5)	1a	68
2		1b	65
3		1c	78
4		IMes	42
5	H (5.0)	1c	93
6	Ph (5.0)	1c	>99 (α:γ = 48:52)

	X	Y	Z
9c	C$_6$F$_5$	C$_6$F$_5$	Br
10c	Br	C$_6$F$_5$	C$_6$F$_5$
11c	Br	C$_6$F$_5$	Br
12c	Br	Br	C$_6$F$_5$
13c	Br	Br	Br
14c	Br	O^{t}Bu	Br

Figure 7. (A) C−C bond formation between allyl bromide and Al(C$_6$F$_5$)$_3$(tol)$_{0.5}$. Yield and the ratio of α/γ substitution were determined by GC analysis. (B) Stepwise transformation of **2c**. Structures of products (**9c**, **13c**, and **14c**) and possible intermediates (**10c**−**12c**) are also shown. Yield of products was determined by NMR analyses. Isolated yield of (**9c**)$_2$ was given in parentheses. (C) Catalytic C−C bond formation between allyl bromide and Al(C$_6$F$_5$)$_3$ derivatives. The yield of allyl pentafluorobenzene was determined by GC analysis.

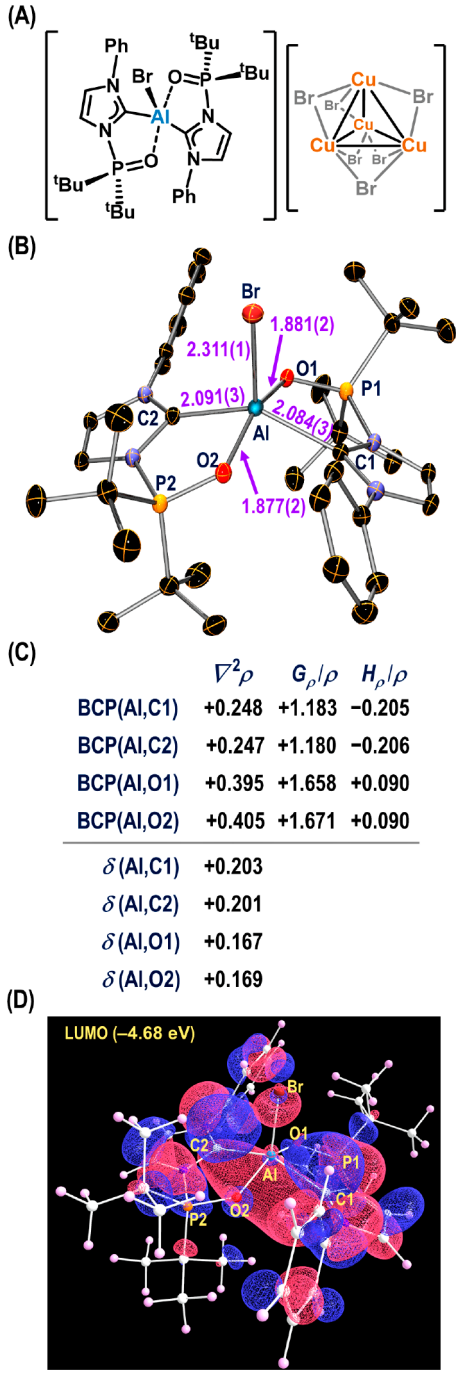

	$\nabla^2\rho$	G_ρ/ρ	H_ρ/ρ
BCP(Al,C1)	+0.248	+1.183	−0.205
BCP(Al,C2)	+0.247	+1.180	−0.206
BCP(Al,O1)	+0.395	+1.658	+0.090
BCP(Al,O2)	+0.405	+1.671	+0.090
δ(Al,C1)	+0.203		
δ(Al,C2)	+0.201		
δ(Al,O1)	+0.167		
δ(Al,O2)	+0.169		

Figure 8. (A) Structure of **15c**. (B) Molecular structure of the cationic unit in **15c** with thermal ellipsoids at 30% probability; H atoms are omitted for clarity. Selected bond lengths (Å) are also shown. (C) The$\nabla^2\rho$ [$e \times r_{Bohr}^{-3}$], G_ρ/ρ, and H_ρ/ρ values at the bond critical points BCP(X,Y) between two atoms (X and Y). Delocalization indices δ(X,Y) are also given on the basis of the SCF density. G_ρ and H_ρ mean the kinetic and the total energy density, respectively, at the corresponding BCP(X,Y). (D) LUMO orbitals and energy level for the cationic unit in **15c**.

not observed. In addition, the thermolysis of (**9c**)$_2$ yielded a complex mixture including HC$_6$F$_5$ and isobutene. DFT calculations predicted that the formation of **10c** from **9c** is endothermic (ΔG° = +4.9 kcal·mol^{-1}), and the observation of the formation of **10c** would thus be difficult under the aforementioned reaction conditions. On the basis of these results, we concluded that heating would be required for the dissociation of dimeric species such as (**9c**)$_2$ and (**11c**)$_2$ into their monomeric form and/or the second/third transmetalation between the Cu−Br and Al−C$_6$F$_5$ units to furnish Cu−C$_6$F$_5$ species such as **10c** and **12c**.

The C−C bond formation between Et$_3$P═O·Al(C$_6$F$_5$)$_3$ and allyl bromide proceeded efficiently in the presence of 20 mol % CuO^{t}Bu and **1c** (i.e., 6.7 mol % with respect to the C$_6$F$_5$ units) to afford allyl pentafluorobenzene in 85% yield. The

https://dx.doi.org/10.1021/jacs.0c03252
J. Am. Chem. Soc. 2020, 142, 9772−9784

oligomerization of allyl bromide was only observable when $Al(C_6F_5)_3(tol)_{0.5}$ was employed. It should be noted here that the treatment of **1c** with $Et_3P{=}O{\cdot}Al(C_6F_5)_3$ resulted in a ligand exchange equilibrium, i.e., **1c** + $Et_3P{=}O{\cdot}Al(C_6F_5)_3$ ⇆ **3c** + $Et_3P{=}O$, indicating that the *in situ* generation of **3c** is possible under the presented reaction conditions.[8] Nevertheless, the details of the reaction mechanism underlying this catalytic synthesis of allyl pentafluorobenzene remain unclear at this point.

We also evaluated the molecular structure of **15c** (Figure 8). A single-crystal X-ray diffraction analysis unambiguously revealed the molecular structure of the cationic part of **15c**, which contains a pentacoordinated dicationic Al(III) species in which two molecules of **1c** coordinate to the Al center in a *κ-C,O* fashion (Figure 8B). The two **1c** units in the solid-state structure of the $[(\kappa\text{-}C,O\text{-}\mathbf{1c})_2AlBr]^+$ moiety exhibit nearly identical bonding situations, which was reproduced in the DFT optimized gas-phase structure, i.e., bond lengths (Å) in the crystalline state (in the gas-phase structure at the ωB97X-D/6-311g(d,p)//6-31g(d,p) level of theory): Al−C1 = 2.084(3) (2.08); Al−C2 = 2.091(3) (2.07); Al−O1 = 1.881(2) (1.91); Al−O2 = 1.877(2) (1.91). In addition, the bonding situation in these **1c** units is almost identical to that in free **1c**. The electronic structure of $[(\kappa\text{-}C,O\text{-}\mathbf{1c})_2AlBr]^+$ was then evaluated in terms of $\nabla^2\rho$ ($e \times r_{Bohr}^{-3}$), G_ρ/ρ, and H_ρ/ρ values at the bond critical point BCP(X,Y) between two atoms (X and Y), on the basis of the AIM analysis using the aforementioned optimized gas-phase structure (Figure 8C). The total energy density (H_ρ, he^{-1}), which is given as the sum of the kinetic energy density (G_ρ, he^{-1}) and the potential energy density (V_ρ, he^{-1}), tends to exhibit a negative value at a bond critical point of a covalent bond and a M−L interaction, i.e., H_ρ(covalent) ≪ H_ρ(M−L) < 0.[14] Moreover, an increased covalency tends to give a value of $G_\rho/\rho < 1$ at a bond critical point, while a value of $G_\rho/\rho \approx 1$ is expected for a M−L interaction. On the other hand, an excess of G_ρ, which can be observed at the bond critical point of ionic or noncovalent interactions, causes the separation of the interatomic surface, resulting in $H_\rho > 0$ and $G_\rho/\rho > 1$. As shown in Figure 8C, $H_\rho < 0$ and $G_\rho/\rho \approx 1$ are obtained at BCP(Al,C1) and BCP(Al,C2), demonstrating a participation of donor−acceptor interactions between the Lewis-basic carbene atoms (C1 and C2) and the Lewis-acidic $Al(III)^{2+}$ center. The cationic charges can thus be expected to be localized mainly on the Al atom (not on imidazolium rings) in the $[(\kappa\text{-}C,O\text{-}\mathbf{1c})_2AlBr]^+$ moiety, which is consistent with the obtained values of $\nabla^2\rho$ and δ(X,Y) as well as the results of an NBO analysis.[8] The results of $H_\rho > 0$ and $G_\rho/\rho > 1$ at BCP(Al,O1) and BCP(Al,O2) would suggest an involvement of noncovalent interactions between the phosphinoyl oxygen atoms (O1 and O2) and the Al atom. Examples of isolated mononuclear dicationic Al(III) species are very rare,[17] and to the best of our knowledge, **15c** includes the first example of a pentacoordinated mononuclear dicationic Al(III) species. The LUMO in the $[(\kappa\text{-}C,O\text{-}\mathbf{1c})_2AlBr]^+$ unit represents the in-phase overlap of the p orbitals on the two carbene carbon (C1 and C2) and Al atoms (Figure 8D).

CONCLUSIONS

We have synthesized heterobimetallic Cu/Al complexes that bear *N*-phosphine-oxide-substituted imidazolylidenes (PoxIms), in which the spatial separation or approximation of Cu and Al fragments can be effectively controlled by rotation of the *N*-phosphinoyl group. Transmetalation to exchange the Cu−O^{t}Bu and Al−C_6F_5 bonds in such heterobimetallic PoxIm complexes leads to the formation of Cu−C_6F_5 and Al−O^{t}Bu bonds in excellent yield. The results of mechanistic studies suggest that this transmetalation determines the reaction rate and predominantly occurs via a key transition state that includes the coordination of the phosphinoyl oxygen atom to both the Cu and Al centers. The critical role of the *N*-phosphinoyl moiety in this transmetalation can thus be identified as (i) the stabilization of the cationic Cu center; (ii) the effective activation of $Al(C_6F_5)_3$; (iii) the construction of a preferable and approachable arrangement of the Al−C_6F_5 units with respect to Cu−O^{t}Bu. Furthermore, we have demonstrated the formation of C−C bonds between allyl bromide and $Al(C_6F_5)_3$ mediated/catalyzed by heterobimetallic Cu/Al complexes that bear PoxIm ligands. The structure of a monomeric pentacoordinated dicationic Al(III) complex, generated as a byproduct in the aforementioned C−C bond formation reactions, was fully characterized. In their entirety, the results presented in this study describe an effective strategy to expand the utility of the heterobimetallic complexes that bear multifunctional carbenes by not only designing molecular structures but also controlling molecular motions.

EXPERIMENTAL SECTION

General Considerations for the Experimental Conditions. Unless otherwise noted, all manipulations were conducted under a nitrogen atmosphere using standard Schlenk line or drybox techniques. All commercially available reagents, including super-dehydrated solvents (toluene, hexane, and CH_2Cl_2), were used as received. Benzene-d_6 and toluene-d_8 were distilled from sodium benzophenone ketyl prior to use. CD_2Cl_2 and CD_3CN were distilled from CaH_2 and stored over molecular sieves (4 Å). (S)PoxIms **1a−c** and $Al(C_6F_5)_3(tol)_{0.5}$ were prepared using previously reported procedures.[4,18] *Caution: $Al(C_6F_5)_3$ is a potentially explosive material, and ligand-supported derivatives such as $Al(C_6F_5)_3(tol)_{0.5}$ should thus be handled with the utmost care.*

Synthesis of 2a from 1a. $Al(C_6F_5)_3(tol)_{0.5}$ (57.4 mg, 0.10 mmol) and CuO^{t}Bu (13.7 mg, 0.10 mmol) were sequentially added to a toluene solution of **1a** (38.9 mg, 0.10 mmol, 0.005 M) at −30 °C. After 30 min of stirring at this temperature, the reaction mixture was allowed to warm to room temperature, where it was stirred for a further 1 h. After the removal of all volatiles *in vacuo*, the residue was washed with cool hexane to give **2a** as a white solid (107.0 mg, 0.10 mmol, >99%). A single crystal was prepared by recrystallization from toluene/hexane at −35 °C. ^{1}H NMR (400 MHz, CD_2Cl_2): δ 9.09 (t, J = 2.4 Hz, 1H, Im-*H*), 7.55 (t, J = 8.0 Hz, 1H, Ar-*H*), 7.34 (d, J = 8.0 Hz, 2H, Ar-*H*), 7.31 (t, J = 1.0 Hz, 1H, Im-*H*), 2.38−2.31 (m, 2H, C*H*CH$_3$), 1.57 (d, $^3J_{H,P}$ = 17.6 Hz, 18H, ^{t}Bu-*H*), 1.26 (d, J = 6.8 Hz, 6H, CHC*H*$_3$), 1.24 (s, 9H, O^{t}Bu-*H*), 1.21 (d, J = 6.8 Hz, 6H, CHC*H*$_3$). ^{13}C{^{1}H} NMR (100 MHz, CD_2Cl_2): δ 183.9 (d, $^2J_{C,P}$ = 20.0 Hz, NCN), 150.1 (dm, $^1J_{C,F}$ = 230 Hz), 145.7, 141.5 (dm, $^1J_{C,F}$ = 250 Hz), 137.1 (dm, $^1J_{C,F}$ = 251 Hz), 136.2 (dm, $^1J_{C,F}$ = 249 Hz), 134.0, 131.5, 127.2, 124.8, 123.7 (d, J = 5.0 Hz), 70.1, 38.9 (d, $^1J_{C,P}$ = 58.0 Hz), 33.2 (d, J = 6.0 Hz), 29.3 (d, J = 5.0 Hz), 26.8 (d, J = 6.0 Hz), 24.4 (d, J = 6.0 Hz), 24.1 (d, J = 7.0 Hz). Several resonances for the C_6F_5 ring were not observed. ^{19}F NMR (376 MHz, CD_2Cl_2): δ −116.2 (m, 2F), −125.1 (m, 4F), −158.4 (t, J = 18.8 Hz, 2F), −163.7 (t, J = 18.8 Hz, 1F), −165.9 (m, 4F), −167.0 (m, 2F). ^{27}Al NMR (103 MHz, CD_2Cl_2): δ 96.5 (bs). ^{31}P{^{1}H} NMR (162 MHz, CD_2Cl_2): δ 84.0 (s). Accurate elemental analyses of **2a** were precluded by extreme air or thermal sensitivity and/or systematic problems. Anal. Calcd for $C_{45}H_{46}AlCuF_{15}N_2O_2P$: C, 51.31; H, 4.40; N, 2.66. Found: C, 50.77; H, 4.76; N, 2.87. X-ray data for **2a**: M = 1053.36, colorless, triclinic, $P\bar{1}$ (#2), a = 10.7445(2) Å, b = 13.4502(2) Å, c = 21.5779(3) Å, α = 102.0818(14)°, β = 99.1286(14)°, γ = 109.5393(16)°, V = 2783.81(9) Å^3, Z = 2, D_{calcd} = 1.257 g/cm^3, T = −150 °C, R_1 ($_wR_2$) = 0.0417 (0.1194).

https://dx.doi.org/10.1021/jacs.0c03252
J. Am. Chem. Soc. 2020, 142, 9772−9784

Synthesis of 3a. $Al(C_6F_5)_3(tol)_{0.5}$ (29.4 mg, 0.051 mmol) was added to a toluene solution of **1a** (19.9 mg, 0.051 mmol, 0.01 M) at −30 °C. The reaction mixture was initially stirred at this temperature and then allowed to warm to room temperature for 1 h. After the removal of all volatiles *in vacuo*, the residue was washed with cold hexane to give **3a** as a white solid (45.9 mg, 0.050 mmol, 98%). A single crystal was prepared by recrystallization from toluene/hexane at −35 °C. ^{1}H NMR (400 MHz, CD_2Cl_2, −30 °C): δ 7.49 (brs, 1H, Im-*H*), 7.45 (t, J = 7.6 Hz, 1H, Ar-*H*), 7.28 (d, J = 7.6 Hz, 2H, Ar-*H*), 7.09 (brs, 1H, Im-*H*), 2.40−2.33 (m, 2H, C*H*CH$_3$), 1.34 (d, $^3J_{H,P}$ = 17.2 Hz, 18H, ^{t}Bu-*H*), 1.14 (d, J = 6.8 Hz, 6H, CHC*H*$_3$), 1.08 (d, J = 6.8 Hz, 6H, CHC*H*$_3$). ^{13}C{^{1}H} NMR (100 MHz, CD_2Cl_2, −30 °C): δ 220.9 (d, $^2J_{C,P}$ = 34.8 Hz, NCN), 149.8 (dm, $^1J_{C,F}$ = 231 Hz), 145.5, 141.2 (dm, $^1J_{C,F}$ = 245 Hz), 136.6 (dm, $^1J_{C,F}$ = 249 Hz), 136.2, 129.7, 123.9, 123.0, 122.3, 38.5 (d, $^1J_{C,P}$ = 61.5 Hz), 28.4, 25.9, 24.1, 23.3. Resonances for the *ipso*-carbons of the C_6F_5 ring were not observed. ^{19}F NMR (376 MHz, CD_2Cl_2, −30 °C): δ −121.4 (d, J = 22.9 Hz, 6F), −154.1 (t, J = 22.9 Hz, 3F), −162.3 (brs, 6F). ^{27}Al NMR (103 MHz, CD_2Cl_2, −30 °C): δ 117.2 (brs). ^{31}P{^{1}H} NMR (162 MHz, CD_2Cl_2, −30 °C): δ 80.5 (s). Anal. Calcd for $C_{41}H_{37}AlF_{15}N_2OP$: C, 53.72; H, 4.07; N, 3.06. Found: C, 53.52; H, 4.05; N, 3.23. X-ray data for **3a**·C_7H_8: M = 1008.84, colorless, triclinic, $P\bar{1}$ (#2), a = 10.6515(3) Å, b = 12.2115(3) Å, c = 18.7731(5) Å, α = 77.285(2)°, β = 87.441(2)°, γ = 77.196(2)°, V = 2322.70(11) Å^3, Z = 2, D_{calcd} = 1.442 g/cm^3, T = −150 °C, R_1 ($_wR_2$) = 0.0507 (0.1431).

Synthesis of 4a. CuO^tBu (13.7 mg, 0.10 mmol) was added to a toluene solution of **1a** (38.9 mg, 0.10 mmol, 0.01 M). The reaction mixture was stirred at room temperature for 1 h. After the removal of all volatiles *in vacuo*, the residue was washed with cold hexane to give **4a** as a white solid (51.7 mg, 0.098 mmol, 98%). A single crystal was prepared by recrystallization from THF/hexane at −35 °C. ^{1}H NMR (400 MHz, C_6D_6): δ 7.73 (t, J = 1.8 Hz, 1H, Im-*H*), 7.24 (t, J = 8.0 Hz, 1H, Ar-*H*), 7.08 (d, J = 8.0 Hz, 2H, Ar-*H*), 6.23 (d, J = 1.8 Hz, 1H, Im-*H*), 2.45−2.38 (m, 2H, C*H*CH$_3$), 1.43 (d, J = 7.0 Hz, 6H, CHC*H*$_3$), 1.38 (d, $^3J_{H,P}$ = 15.2 Hz, 18H, ^{t}Bu-*H*), 1.35 (s, 9H, O^{t}Bu-*H*), 0.98 (d, J = 7.0 Hz, 6H, CHC*H*$_3$). ^{13}C{^{1}H} NMR (100 MHz, C_6D_6): δ 183.5 (d, $^2J_{C,P}$ = 11.0 Hz, NCN), 145.6, 135.8, 130.5, 124.4, 121.39, 121.35, 69.2, 37.9 (d, $^1J_{C,P}$ = 65.0 Hz), 37.3, 28.9, 27.3, 24.4, 24.3. ^{31}P{^{1}H} NMR (162 MHz, C_6D_6): δ 68.2 (s). Anal. Calcd for $C_{27}H_{46}CuN_2O_2P$: C, 61.75; H, 8.88; N, 5.33. Found: C, 61.4; H, 9.18; N, 5.32. X-ray data for (**4a**·THF)$_2$: M = 1194.61, colorless, orthorhombic, $Pna2_1$ (#33), a = 23.7593(3) Å, b = 13.3807(2) Å, c = 21.4965(3) Å, α = 90°, β = 90°, γ = 90°, V = 6834.08(16) Å^3, Z = 4, D_{calcd} = 1.161 g/cm^3, T = −150 °C, R_1 ($_wR_2$) = 0.0805 (0.2845).

Synthesis of 8a. Complex **3a** (91.7 mg, 0.10 mmol) was added to a 1,2-dichloroethane solution of **4a** (52.5 mg, 0.10 mmol, 0.03 M). The reaction mixture was stirred at room temperature for 1 h. After the removal of all volatiles *in vacuo*, the residue was washed with cold hexane to afford **8a** as a white solid (134.1 mg, 0.093 mmol, 93%). A single crystal was prepared by recrystallization from toluene/hexane at −35 °C. ^{1}H NMR (400 MHz, CD_2Cl_2): δ 7.36 (t, J = 8.0 Hz, 2H, Ar-*H*), 7.25 (d, J = 0.8 Hz, 2H, Im-*H*), 7.16 (d, J = 8.0 Hz, 4H, Ar-*H*), 7.05 (s, 2H, Im-*H*), 2.38−2.31 (m, 4H, C*H*CH$_3$), 1.28 (d, J = 15.2 Hz, 36H, ^{t}Bu-*H*), 1.14 (s, 9H, O^{t}Bu-*H*), 0.99 (d, J = 6.8 Hz, 12H, CHC*H*$_3$), 0.90 (d, J = 6.8 Hz, 12H, CHC*H*$_3$). ^{13}C{^{1}H} NMR (100 MHz, CD_2Cl_2): δ 190.3 (d, $^2J_{C,P}$ = 12.0 Hz, NCN), 150.1 (dm, $^1J_{C,F}$ = 228 Hz), 145.7, 140.1 (dm, $^1J_{C,F}$ = 241 Hz), 136.6 (dm, $^1J_{C,F}$ = 243 Hz), 136.2, 130.5, 126.8 (d, J = 4.0 Hz), 124.3, 120.0 (d, J = 4.0 Hz), 68.7, 37.5 (d, $^1J_{C,P}$ = 65.0 Hz), 33.3, 28.7, 26.7, 24.3, 23.9. Resonances for the *ipso* carbons of the C_6F_5 ring were not identified. ^{19}F NMR (376 MHz, CD_2Cl_2): δ −125.5 (d, J = 18.8 Hz, 6F), −163.1 (t, J = 18.8 Hz, 3F), −168.3 (m, 6F). ^{27}Al NMR (103 MHz, CD_2Cl_2): δ 96.9 (s). ^{31}P{^{1}H} NMR (162 MHz, CD_2Cl_2): δ 64.5 (s). HRMS (FAB$^+$): m/z Calcd for $C_{46}H_{74}N_4O_2P_2Cu$: ([(**1a**)$_2$Cu$^+$]) 839.4583, Found 839.4600. X-ray data for **8a**: M = 1441.89, colorless, orthorhombic, *Pbca* (#61), a = 19.1617(2) Å, b = 19.1616(2) Å, c = 38.3323(4) Å, α = 90°, β = 90°, γ = 90°, V = 14074.4(3) Å^3, Z = 8, D_{calcd} = 1.744 g/cm^3, T = −150 °C, R_1 ($_wR_2$) = 0.0410 (0.1054).

■ ASSOCIATED CONTENT

Supporting Information

The Supporting Information is available free of charge at https://pubs.acs.org/doi/10.1021/jacs.0c03252.

Full details pertaining to the experimental methods, identification of the compounds, DFT calculations, and NMR spectra (PDF)

CIF data for **2a**−**2c**, **3a**, **3b**, **4a**, **5a**, **5b**, **8a**, **9c**, **15c**, $Et_3P{=}O{\cdot}Al(C_6F_5)$ and [IMesCu(μ-O^{t}Bu)Al(C_6F_5)$_3$] (CIF)

■ AUTHOR INFORMATION

Corresponding Authors

Yoichi Hoshimoto − *Department of Applied Chemistry, Faculty of Engineering, Osaka University, Suita, Osaka 565-0871, Japan*; orcid.org/0000-0003-0882-6109; Email: hoshimoto@chem.eng.osaka-u.ac.jp

Sensuke Ogoshi − *Department of Applied Chemistry, Faculty of Engineering, Osaka University, Suita, Osaka 565-0871, Japan*; orcid.org/0000-0003-4188-8555; Email: ogoshi@chem.eng.osaka-u.ac.jp

Author

Takahiro Asada − *Department of Applied Chemistry, Faculty of Engineering, Osaka University, Suita, Osaka 565-0871, Japan*

Complete contact information is available at: https://pubs.acs.org/10.1021/jacs.0c03252

Notes

The authors declare no competing financial interest.

■ ACKNOWLEDGMENTS

This work was supported by a Grant-in-Aid for Young Scientists (JSPS KAKENHI grant JP18K14219) and the Grant-in-Aid for Scientific Research on Innovative Areas "Precisely Designed Catalysts with Customized Scaffolding (JSPS KAKENHI grant JP15H05803)." Y.H. acknowledges valuable suggestions on the theoretical studies from Prof. Atsushi Tahara (Kyusyu University). T.A. expresses his special thanks for a Grant-in-Aid for JSPS Fellows.

■ REFERENCES

(1) For selected books, see: (a) Nolan, S. P., Ed. *N-Heterocyclic Carbenes in Synthesis*; Wiley-VCH: Weinheim, 2006. (b) Glorius, F., Ed. *N-Heterocyclic Carbenes in Transition Metal Catalysis*; Springer: Berlin, 2007. (c) Cazin, C. S. J., Ed. *N-Heterocyclic Carbenes in Transition Metal Catalysis and Organocatalysis*; Springer: Netherlands, 2011. For selected reviews, see: (d) Hahn, F. E.; Jahnke, M. C. Heterocyclic Carbenes: Synthesis and Coordination Chemistry. *Angew. Chem., Int. Ed.* **2008**, *47*, 3122−3172. (e) De Frémont, P.; Marion, N.; Nolan, S. P. Carbenes: Synthesis, Properties, and Organometallic Chemistry. *Coord. Chem. Rev.* **2009**, *253*, 862−892. (f) Melaimi, M.; Soleilhavoup, M.; Bertrand, G. Stable Cyclic Carbenes and Related Species beyond Diaminocarbenes. *Angew. Chem., Int. Ed.* **2010**, *49*, 8810−8849. (g) Wang, Y.; Robinson, G. H. Carbene-Stabilized Main Group Diatomic Allotropes. *Dalton Trans.* **2012**, *41*, 337−345. (h) Nelson, D. J.; Nolan, S. P. Quantifying and Understanding the Electronic Properties of *N*-Heterocyclic Carbenes. *Chem. Soc. Rev.* **2013**, *42*, 6723−6753. (i) Hopkinson, M. N.; Richter, C.; Schedler, M.; Glorius, F. An Overview of *N*-Heterocyclic Carbenes. *Nature* **2014**, *510*, 485−496. (j) Flanigan, D. M.; Romanov-Michailidis, F.; White, N. A.; Rovis, T. Organocatalytic Reactions Enabled by *N*-Heterocyclic Carbenes. *Chem. Rev.* **2015**, *115*, 9307−9387. (k) Gómez-Suárez, A.; Nelson, D. J.; Nolan, S. P.

Quantifying and Understanding the Steric Properties of *N*-Heterocyclic Carbenes. *Chem. Commun.* **2017**, *53*, 2650−2660. (l) Nesterov, V.; Reiter, D.; Bag, P.; Frisch, P.; Holzner, R.; Porzelt, A.; Inoue, S. NHCs in Main Group Chemistry. *Chem. Rev.* **2018**, *118*, 9678−9842. (m) Smith, C. A.; Narouz, M. R.; Lummis, P. A.; Singh, I.; Nazemi, A.; Li, C. H.; Crudden, C. M. *N*-Heterocyclic Carbenes in Materials Chemistry. *Chem. Rev.* **2019**, *119*, 4986−5056.

(2) For selected reviews, see: (a) Kühl, O. The Chemistry of Functionalised *N*-Heterocyclic Carbenes. *Chem. Soc. Rev.* **2007**, *36*, 592−607. (b) Liddle, S. T.; Edworthy, I. S.; Arnold, P. L. Anionic Tethered *N*-Heterocyclic Carbene Chemistry. *Chem. Soc. Rev.* **2007**, *36*, 1732−1744. (c) Normand, A. T.; Cavell, K. J. Donor-Functionalised *N*-Heterocyclic Carbene Complexes of Group 9 and 10 Metals in Catalysis: Trends and Directions. *Eur. J. Inorg. Chem.* **2008**, *2008*, 2781−2800. (d) Mercs, L.; Albrecht, M. Beyond Catalysis: *N*-Heterocyclic Carbene Complexes as Components for Medicinal, Luminescent, and Functional Materials Applications. *Chem. Soc. Rev.* **2010**, *39*, 1903−1912. (e) Gaillard, S.; Renaud, J. L. When Phosphorus and NHC (*N*-Heterocyclic Carbene) Meet Each Other. *Dalton Trans.* **2013**, *42*, 7255−7270. (f) Fliedel, C.; Braunstein, P. Recent Advances in *S*-Functionalized *N*-Heterocyclic Carbene Ligands: From the Synthesis of Azolium Salts and Metal Complexes to Applications. *J. Organomet. Chem.* **2014**, *751*, 286−300. (g) Mata, J. A.; Hahn, F. E.; Peris, E. Heterometallic Complexes, Tandem Catalysis and Catalytic Cooperativity. *Chem. Sci.* **2014**, *5*, 1723−1732. (h) Hameury, S.; De Frémont, P.; Braunstein, P. Metal Complexes with Oxygen-Functionalized NHC Ligands: Synthesis and Applications. *Chem. Soc. Rev.* **2017**, *46*, 632−733. (i) Hazra, S.; Hoshimoto, Y.; Ogoshi, S. *N*-Phosphine Oxide-Substituted Imidazolylidenes (PoxIms): Multifunctional Multipurpose Carbenes. *Chem. - Eur. J.* **2017**, *23*, 15238−15243. (j) Vivancos, Á.; Segarra, C.; Albrecht, M. Mesoionic and Related Less Heteroatom-Stabilized *N*-Heterocyclic Carbene Complexes: Synthesis, Catalysis, and Other Applications. *Chem. Rev.* **2018**, *118*, 9493−9586. (k) Kuwata, S.; Hahn, F. E. Complexes Bearing Protic *N*-Heterocyclic Carbene Ligands. *Chem. Rev.* **2018**, *118*, 9642−9677. (l) Peris, E. Smart *N*-Heterocyclic Carbene Ligands in Catalysis. *Chem. Rev.* **2018**, *118*, 9988−10031. (m) Danopoulos, A. A.; Simler, T.; Braunstein, P. *N*-Heterocyclic Carbene Complexes of Copper, Nickel, and Cobalt. *Chem. Rev.* **2019**, *119*, 3730−3961. (n) Doddi, A.; Peters, M.; Tamm, M. *N*-Heterocyclic Carbene Adducts of Main Group Elements and Their Use as Ligands in Transition Metal Chemistry. *Chem. Rev.* **2019**, *119*, 6994−7112.

(3) (a) Arduengo, A. J., III; Tapu, D.; Marshall, W. J. A Bimetallic Complex Containing a Cyclopentadienyl-Annulated Imidazol-2-Ylidene. *J. Am. Chem. Soc.* **2005**, *127*, 16400−16401. (b) Mas-Marzá, E.; Mata, J. A.; Peris, E. Triazolediylidenes: A Versatile Class of Ligands for the Preparation of Discrete Molecules of Homo- and Hetero-Binuclear Complexes for Improved Catalytic Applications. *Angew. Chem., Int. Ed.* **2007**, *46*, 3729−3731. (c) Zhou, Y.; Xi, Z.; Chen, W.; Wang, D. Dinickel(II) Complexes of Bis(*N*-Heterocyclic Carbene) Ligands Containing $[Ni_2(\mu\text{-}OH)]$ Cores as Highly Efficient Catalysts for the Coupling of Aryl Chlorides. *Organometallics* **2008**, *27*, 5911−5920. (d) Zanardi, A.; Mata, J. A.; Peris, E. Well-Defined Ir/Pd Complexes with a Triazolyl-Diylidene Bridge as Catalysts for Multiple Tandem Reactions. *J. Am. Chem. Soc.* **2009**, *131*, 14531−14537. (e) Mendoza-Espinosa, D.; Donnadieu, B.; Bertrand, G. Facile Preparation of Homo- and Hetero-Dimetallic Complexes with a 4-Phosphino-Substituted NHC Ligand. Toward the Design of Multifunctional Catalysts. *Chem. - Asian J.* **2011**, *6*, 1099−1103. (f) Gu, S.; Xu, D.; Chen, W. Heterobimetallic Complexes Containing an *N*-Heterocyclic Carbene Based Multidentate Ligand and Catalyzed Tandem Click/Sonogashira Reactions. *Dalton Trans.* **2011**, *40*, 1576−1583. (g) Ruiz, J.; Mesa, A. F. A 4,5-Diphosphino-Substituted Imidazolium Salt: A Building Block for the Modular Synthesis of Mixed Diphosphine-NHC Heterometallic Complexes. *Chem. - Eur. J.* **2012**, *18*, 4485−4488. (h) Maity, R.; Koppetz, H.; Hepp, A.; Hahn, F. E. Heterobimetallic Carbene Complexes by a Single-Step Site-Selective Metalation of a Tricarbene Ligand. *J. Am. Chem. Soc.* **2013**, *135*, 4966−4969. (i) Majhi, P. K.; Serin, S. C.; Schnakenburg, G.; Gates, D. P.; Streubel, R. Mono- and Hetero-Dinuclear Complexes of Janus-Head NHC Ligands Possessing Backbone Phosphinoyl Groups: The Case of Soft and Hard Metal Centers. *Eur. J. Inorg. Chem.* **2014**, *2014*, 4975−4983. (j) Simler, T.; Braunstein, P.; Danopoulos, A. A. Relative Lability and Chemoselective Transmetallation of NHC in Hybrid Phosphine-NHC Ligands: Access to Heterometallic Complexes. *Angew. Chem., Int. Ed.* **2015**, *54*, 13691−13695. (k) Simler, T.; Braunstein, P.; Danopoulos, A. A. Coinage Metal Complexes with Bridging Hybrid Phosphine-NHC Ligands: Synthesis of Di- and Tetra-Nuclear Complexes. *Dalton Trans.* **2016**, *45*, 5122−5139. (l) Gonell, S.; Poyatos, M.; Peris, E. Pincer-CNC Mononuclear, Dinuclear and Heterodinuclear Au(III) and Pt(II) Complexes Supported by Mono- and Poly-*N*-Heterocyclic Carbenes: Synthesis and Photophysical Properties. *Dalton Trans.* **2016**, *45*, 5549−5556. (m) Sinha, N.; Hahn, F. E. Metallosupramolecular Architectures Obtained from Poly-*N*-Heterocyclic Carbene Ligands. *Acc. Chem. Res.* **2017**, *50*, 2167−2184. (n) Ai, P.; Monakhov, K. Y.; van Leusen, J.; Kögerler, P.; Gourlaouen, C.; Tromp, M.; Welter, R.; Danopoulos, A. A.; Braunstein, P. Linear $Cu^{I}_{2}Pd^{0}$, $Cu^{I}Pd^{0}_{2}$, and $Ag^{I}_{2}Pd^{0}$ Metal Chains Supported by Rigid *N,N′*-Diphosphanyl *N*-Heterocyclic Carbene Ligands and Metallophilic Interactions. *Chem. - Eur. J.* **2018**, *24*, 8787−8796. (o) Srivastava, R.; Moneuse, R.; Petit, J.; Pavard, P.-A.; Dardun, V.; Rivat, M.; Schiltz, P.; Solari, M.; Jeanneau, E.; Veyre, L.; Thieuleux, C.; Quadrelli, E. A.; Camp, C. Early/Late Heterobimetallic Tantalum/Rhodium Species Assembled Through a Novel Bifunctional NHC-OH Ligand. *Chem. - Eur. J.* **2018**, *24*, 4361−4370.

(4) (a) Hoshimoto, Y.; Kinoshita, T.; Ohashi, M.; Ogoshi, S. A Strategy to Control the Reactivation of Frustrated Lewis Pairs from Shelf-Stable Carbene Borane Complexes. *Angew. Chem., Int. Ed.* **2015**, *54*, 11666−11671. (b) Hoshimoto, Y.; Asada, T.; Hazra, S.; Kinoshita, T.; Sombut, P.; Kumar, R.; Ohashi, M.; Ogoshi, S. Strategic Utilization of Multifunctional Carbene for Direct Synthesis of Carboxylic−Phosphinic Mixed Anhydride from CO_2. *Angew. Chem., Int. Ed.* **2016**, *55*, 16075−16079. (c) Hoshimoto, Y.; Asada, T.; Hazra, S.; Ohashi, M.; Ogoshi, S. Phosphorylation of Isocyanates and Aldehydes Mediated by Multifunctional *N*-Phosphine Oxide-Substituted Imidazolylidenes. *Chem. Lett.* **2017**, *46*, 1211−1213. (d) Tao, W.; Akita, S.; Nakano, R.; Ito, S.; Hoshimoto, Y.; Ogoshi, S.; Nozaki, K. Copolymerisation of Ethylene with Polar Monomers by Using Palladium Catalysts Bearing an *N*-Heterocyclic Carbene-Phosphine Oxide Bidentate Ligand. *Chem. Commun.* **2017**, *53*, 2630−2633. (e) Kinoshita, T.; Sakuraba, M.; Hoshimoto, Y.; Ogoshi, S. Complexation between MOTf (M = Li and Na) and *N*-Phosphine Oxide-Substituted Imidazolylidenes via Coordination of the *N*-Phosphoryl Groups. *Chem. Lett.* **2019**, *48*, 230−233. (f) Branzi, L.; Franco, D.; Baron, M.; Armelao, L.; Rancan, M.; Sgarbossa, P.; Biffis, A. Palladium(II) Complexes with *N*-Phosphine Oxide-Substituted Imidazolylidenes (PoxIms): Coordination Chemistry and Catalysis. *Organometallics* **2019**, *38*, 2298−2306. (g) Branzi, L.; Baron, M.; Armelao, L.; Rancan, M.; Sgarbossa, P.; Graiff, C.; Pöthig, A.; Biffis, A. Coordination Chemistry of Gold with: *N* -Phosphine Oxide-Substituted Imidazolylidenes (PoxIms). *New J. Chem.* **2019**, *43*, 17275−17283. (h) Asada, T.; Hoshimoto, Y.; Kawakita, T.; Kinoshita, T.; Ogoshi, S. Axial Chirality around N-P Bonds Induced by Complexation between $E(C_6F_5)_3$ (E = B, Al) and an *N*-Phosphine Oxide-Substituted Imidazolinylidene: A Key Intermediate in the Catalytic Phosphinoylation of CO_2. *J. Org. Chem.* **2020**, DOI: 10.1021/acs.joc.9b03210.

(5) Cordero, B.; Gómez, V.; Platero-Prats, A. E.; Revés, M.; Echeverría, J.; Cremades, E.; Barragán, F.; Alvarez, S. Covalent Radii Revisited. *Dalton Trans.* **2008**, 2832−2838.

(6) (a) Ho, T.-L. The Hard Soft Acids Bases (HSAB) Principle and Organic Chemistry. *Chem. Rev.* **1975**, *75*, 1−20. (b) Stahl, N. G.; Salata, M. R.; Marks, T. J. $B(C_6F_5)_3$- vs $Al(C_6F_5)_3$-Derived Metallocenium Ion Pairs. Structural, Thermochemical, and Structural Dynamic Divergences. *J. Am. Chem. Soc.* **2005**, *127*, 10898−10909. (c) Timoshkin, A. Y.; Frenking, G. Gas-Phase Lewis Acidity of

https://dx.doi.org/10.1021/jacs.0c03252
J. Am. Chem. Soc. 2020, 142, 9772−9784

Perfluoroaryl Derivatives of Group 13 Elements. *Organometallics* **2008**, *27*, 371−380. (d) Robinson, G. H.; Lee, B.; Pennington, W. T.; Sangokoya, S. A. Facile Cleavage of C-H Bonds. Reaction of Trimethylaluminum with Bis(Diphenylphosphinoyl)Methane: Synthesis and Molecular Structure of $[Al(CH_3)][(C_6H_5)_2P(O)CP(O)(C_6H_5)_2]_2[Al(CH_3)_2]_2$. *J. Am. Chem. Soc.* **1988**, *110*, 6260−6261. (e) Feher, F. J.; Budzichowski, T. A.; Weller, K. J. Polyhedral Aluminosilsesquioxanes: Soluble Organic Analogues of Aluminosilicates. *J. Am. Chem. Soc.* **1989**, *111*, 7288−7289. (f) Maar, R. R.; Rabiee Kenaree, A.; Zhang, R.; Tao, Y.; Katzman, B. D.; Staroverov, V. N.; Ding, Z.; Gilroy, J. B. Aluminum Complexes of $N_2O_2^{3-}$ Formazanate Ligands Supported by Phosphine Oxide Donors. *Inorg. Chem.* **2017**, *56*, 12436−12447. (g) Dardun, V.; Escomel, L.; Jeanneau, E.; Camp, C. On the Alcoholysis of Alkyl-Aluminum(III) Alkoxy-NHC Derivatives: Reactivity of the Al-Carbene Lewis Pair *versus* Al-Alkyl. *Dalton Trans.* **2018**, *47*, 10429−10433.

(7) (a) Zhang, Y.; Miyake, G. M.; Chen, E. Y.-X. Alane-Based Classical and Frustrated Lewis Pairs in Polymer Synthesis: Rapid Polymerization of MMA and Naturally Renewable Methylene Butyrolactones into High-Molecular-Weight Polymers. *Angew. Chem., Int. Ed.* **2010**, *49*, 10158−10162. (b) Fliedel, C.; Schnee, G.; Avilés, T.; Dagorne, S. Group 13 Metal (Al, Ga, In, Tl) Complexes Supported by Heteroatom-Bonded Carbene Ligands. *Coord. Chem. Rev.* **2014**, *275*, 63−86. (c) Arduengo, A. J., III; Dias, H. V. R.; Calabrese, J. C.; Davidson, F. A Stable Carbene−Alane Adduct. *J. Am. Chem. Soc.* **1992**, *114*, 9724−9725. (d) Romain, C.; Fliedel, C.; Bellemin-Laponnaz, S.; Dagorne, S. NHC Bis-Phenolate Aluminum Chelates: Synthesis, Structure, and Use in Lactide and Trimethylene Carbonate Polymerization. *Organometallics* **2014**, *33*, 5730−5739. (e) Schneider, H.; Hock, A.; Bertermann, R.; Radius, U. Reactivity of NHC Alane Adducts towards *N*-Heterocyclic Carbenes and Cyclic (Alkyl)(Amino)Carbenes: Ring Expansion, Ring Opening, and Al−H Bond Activation. *Chem.-Eur. Chem. - Eur. J.* **2017**, *23*, 12387−12398.

(8) For details on the experimental procedures, crystallographic information, and DFT calculations, see the Supporting Information and CIF file.

(9) (a) Xie, W.; Yoon, J. H.; Chang, S. (NHC)Cu-Catalyzed Mild C-H Amidation of (Hetero)Arenes with Deprotectable Carbamates: Scope and Mechanistic Studies. *J. Am. Chem. Soc.* **2016**, *138*, 12605−12614. (b) Xie, W.; Chang, S. [Cu(NHC)]-Catalyzed C-H Allylation and Alkenylation of Both Electron-Deficient and Electron-Rich (Hetero)Arenes with Allyl Halides. *Angew. Chem., Int. Ed.* **2016**, *55*, 1876−1880.

(10) For selected examples, see: (a) Ménard, G.; Stephan, D. W. CO_2 Reduction via Aluminum Complexes of Ammonia Boranes. *Dalton Trans.* **2013**, *42*, 5447−5453. (b) Liu, L. L.; Cao, L. L.; Shao, Y.; Stephan, D. W. Single Electron Delivery to Lewis Pairs: An Avenue to Anions by Small Molecule Activation. *J. Am. Chem. Soc.* **2017**, *139*, 10062−10071.

(11) For a similar type of transformation on *N*-phosphanyl-substituted *N*-heterocyclic carbenes, see: (a) Marchenko, A. P.; Koidan, H. N.; Huryeva, A. N.; Zarudnitskii, E. V.; Yurchenko, A. A.; Kostyuk, A. N. *N*-Phosphorylated Imidazolium Salts as Precursors to 2- and 5-Phosphorylated Imidazoles and New Imidazol-2-Ylidenes Featuring the PNCN Unit. *J. Org. Chem.* **2010**, *75*, 7141−7145. (b) Marchenko, A.; Koidan, H.; Hurieva, A.; Kurpiieva, O.; Vlasenko, Y.; Kostyuk, A.; Tubaro, C.; Lenarda, A.; Biffis, A.; Graiff, C. *N*-Phosphanyl-Imidazolin-2-Ylidenes: Novel Stable Carbenes as Bidentate Ligands for Late Transition Metals. *J. Organomet. Chem.* **2014**, *771*, 14−23.

(12) (a) Thalladi, V. R.; Weiss, H. C.; Bläser, D.; Boese, R.; Nangia, A.; Desiraju, G. R. C−H···F Interactions in the Crystal Structures of Some Fluorobenzenes. *J. Am. Chem. Soc.* **1998**, *120*, 8702−8710. (b) Vangala, V. R.; Nangia, A.; Lynch, V. M. Interplay of Phenyl-Perfluorophenyl Stacking, C−H···F, C−F···π and F···F Interactions in Some Crystalline Aromatic Azines. *Chem. Commun.* **2002**, 1304−1305.

(13) (a) Bader, R. F. W., Ed. *Atoms in Molecules. A Quantum Theory*; Cambridge University Press: Oxford, 1991. (b) Bader, R. F. W.; Stephens, M. E. Spatial Localization of the Electronic Pair and Number Distributions in Molecules. *J. Am. Chem. Soc.* **1975**, *97*, 7391−7399.

(14) Macchi, P.; Sironi, A. Chemical Bonding in Transition Metal Carbonyl Clusters: Complementary Analysis of Theoretical and Experimental Electron Densities. *Coord. Chem. Rev.* **2003**, *238*−*239*, 383−412.

(15) For selected examples, see: (a) Krause, N., Ed. *Modern Organocopper Chemistry*; Wiley-VCH: Weinheim, 2002. (b) Wipf, P. Transmetalation Reactions in Organocopper Chemistry. *Synthesis* **1993**, *1993* (6), 537−557. (c) Sharma, S.; Oehlschlager, A. C. Scope and Mechanism of Stannylalumination of 1-Alkynes. *J. Org. Chem.* **1989**, *54*, 5064−5073. (d) Wipf, P.; Smitrovich, J. H.; Moon, C. W. Transmetalation Reactions of Alkenylalanes: Copper-Catalyzed Conjugate Addition to Enones. *J. Org. Chem.* **1992**, *57*, 3178−3186. (e) Hawner, C.; Li, K.; Cirriez, V.; Alexakis, A. Copper-Catalyzed Asymmetric Conjugate Addition of Aryl Aluminum Reagents to Trisubstituted Enones: Construction of Aryl-Substituted Quaternary Centers. *Angew. Chem., Int. Ed.* **2008**, *47*, 8211−8214. (f) Gao, F.; Lee, Y.; Mandai, K.; Hoveyda, A. H. Quaternary Carbon Stereogenic Centers through Copper-Catalyzed Enantioselective Allylic Substitutions with Readily Accessible Aryl- or Heteroaryllithium Reagents and Aluminum Chlorides. *Angew. Chem., Int. Ed.* **2010**, *49*, 8370−8374. (g) Blümke, T. D.; Groll, K.; Karaghiosoff, K.; Knochel, P. New Preparation of Benzylic Aluminum and Zinc Organometallics by Direct Insertion of Aluminum Powder. *Org. Lett.* **2011**, *13*, 6440−6443. (h) Dabrowski, J. A.; Villaume, M. T.; Hoveyda, A. H. Enantioselective Synthesis of Quaternary Carbon Stereogenic Centers through Copper-Catalyzed Conjugate Additions of Aryl- and Alkylaluminum Reagents to Acyclic Trisubstituted Enones. *Angew. Chem., Int. Ed.* **2013**, *52*, 8156−8159. (i) Endo, K.; Hamada, D.; Yakeishi, S.; Shibata, T. Effect of Multinuclear Copper/Aluminum Complexes in Highly Asymmetric Conjugate Addition of Trimethylaluminum to Acyclic Enones. *Angew. Chem., Int. Ed.* **2013**, *52*, 606−610. (j) Shrestha, B.; Giri, R. Copper-Catalyzed Arylation of Alkyl Halides with Arylaluminum Reagents. *Beilstein J. Org. Chem.* **2015**, *11*, 2400−2407. (k) Ueno, A.; Takimoto, M.; Wylie, W. N. O.; Nishiura, M.; Ikariya, T.; Hou, Z. Copper-Catalyzed Formal C−H Carboxylation of Aromatic Compounds with Carbon Dioxide through Arylaluminum Intermediates. *Chem. - Asian J.* **2015**, *10*, 1010−1016. (l) Shrestha, B.; Thapa, S.; Gurung, S. K.; Pike, R. A. S.; Giri, R. General Copper-Catalyzed Coupling of Alkyl-, Aryl-, and Alkynylaluminum Reagents with Organohalides. *J. Org. Chem.* **2016**, *81*, 787−802.

(16) For related contributions from other groups, see: (a) Yao, T.; Hirano, K.; Satoh, T.; Miura, M. Stereospecific Copper-Catalyzed C-H Allylation of Electron-Deficient Arenes with Allyl Phosphates. *Angew. Chem., Int. Ed.* **2011**, *50*, 2990−2994. (b) Makida, Y.; Ohmiya, H.; Sawamura, M. Regio- and Stereocontrolled Introduction of Secondary Alkyl Groups to Electron-Deficient Arenes through Copper-Catalyzed Allylic Alkylation. *Angew. Chem., Int. Ed.* **2012**, *51*, 4122−4127.

(17) (a) Vidovic, D.; Findlater, M.; Reeske, G.; Cowley, A. H. Synthesis and Characterization of a β-Diketiminate-Supported Aluminum Dication. *J. Organomet. Chem.* **2007**, *692*, 5683−5686. (b) Cao, L. L.; Daley, E.; Johnstone, T. C.; Stephan, D. W. Cationic Aluminum Hydride Complexes: Reactions of Carbene-Alane Adducts with Trityl-Borate. *Chem. Commun.* **2016**, *52*, 5305−5307.

(18) (a) Lee, C. H.; Lee, S. J.; Park, J. W.; Kim, K. H.; Lee, B. Y.; Oh, J. S. Preparation of $Al(C_6F_5)_3$ and Its Use for the Modification of Methylalumoxane. *J. Mol. Catal. A: Chem.* **1998**, *132*, 231−239. (b) Feng, S.; Roof, G. R.; Chen, E. Y.-X. Tantalum(V)-Based Metallocene, Half-Metallocene, and Non-Metallocene Complexes as Ethylene−1-Octene Copolymerization and Methyl Methacrylate Polymerization Catalysts. *Organometallics* **2002**, *21*, 832−839. (c) Chen, J.; Chen, E. Y.-X. Unsolvated $Al(C_6F_5)_3$: Structural Features and Electronic Interaction with Ferrocene. *Dalton Trans.* **2016**, *45*, 6105−6110.

https://dx.doi.org/10.1021/jacs.0c03252
J. Am. Chem. Soc. 2020, 142, 9772−9784